HOKKAIDO UNIVERSITY

Title	Studies on morphofunctional interactions between epithelial cells composing blood-urine barrier in mice : as a role for immunological gate regulating renal pathology [an abstract of entire text]
Author(s)	MASUM, Md. Abdul
Citation	. ( ) 13498
Issue Date	2019-03-25
Doc URL	http://hdl.handle.net/2115/74771
Type	theses (doctoral - abstract of entire text)
Note	
Note(URL)	https://www.lib.hokudai.ac.jp/dissertations/copy-guides/
File Information	Md_Abdul_MASUM_summary.pdf

Instructions for use

Studies on morphofunctional interactions between epithelial cells composing blood-urine barrier in mice

- as a role for immunological gate regulating renal pathology -

マウス血液－尿関門を担う上皮細胞間相互作用に関する形態機能学的研究

－腎病変を制御する免疫学的ゲートとしての役割－

Md. Abdul Masum

Laboratory of Anatomy

Department of Basic Veterinary Sciences

Faculty of Veterinary Medicine

Hokkaido University, Japan

Abbreviations

AGN: autoimmune glomerulonephritis

Actb: actin beta

BUB: blood-urine barrier

BXSB: BXSB/MpJ

CKD: chronic kidney disease

dsDNA: double strand DNA

EC: endothelial cell

EDTA: ethylenediaminetetra acetic acid

EF: endothelial fenestration

ESRD: end-stage renal disease

GBM: glomerular basement membrane

GLs: glomerular lesions

GN: glomerulonephritis

GTA: glutaraldehyde

Glo.: glomerular

IC: immune-complex

IL-1F6: interleukin-1 family, member 6

Ifnγ: interferon, gamma

Il1b, ILB*: interleukin 1, beta*

Il6: interleukin 6

mRNA: messenger ribonucleic acid

mSEM: modified scanning electron microscopy

NBF: neutral buffered formalin

OsO$_4$: osmium tetraoxide

PAM-H: periodic acid methenamine silver

PAS-H: periodic acid Schiff-hematoxylin

PB: phosphate buffer

PBS: phosphate-buffered saline

PCR: polymerase chain reaction

PFA: paraformaldehyde

PFP: podocyte foot process

PT: proximal tubule

PTC: peritubular capillary

RT-PCR: reverse transcription polymerase chain reaction

sBUN: serum blood urea nitrogen

sCre: serum creatinine

SEM: scanning electron microscopy

SLE: systemic lupus erythematosus

TEC: tubular epithelial cell

TEM: transmission electron microscopy

TILs: tubulointerstitial lesions

Tlr, TLR: toll-like receptor

Tnf, TNF: *tumor necrosis factor*

uACR: urinary albumin-to-creatinine ratio

UUO: unilateral ureteral obstruction

VEGF: vascular endothelial growth factor

Wks: weeks

Wt1: Wilms tumor 1

Yaa: BXSB/MpJ-*Yaa*

Yaa: Y-linked autoimmune acceleration

INDEXES

Preface

The adult kidney filtrates about 76 to 148 mL/min of blood under healthy condition (Soares et al., 2013). However, any defects in such system especially that is associated with chronic kidney disease (CKD) lead to end-stage renal disease (ESRD) which requires dialysis and renal transplantation (Smyth et al., 2014). The increased prevalence of patients with CKD is one of the most serious public health problems throughout the world (Tonelli et al., 2006). Interestingly, it has been estimated that over 19 million people in the United States and approximately 22% of adults in Japan have CKD (Coresh et al., 2003 and Nagata et al., 2010). Furthermore, in veterinary medicine, the number of companion animals suffering from CKD is also increasing because of their aging, especially approximately 30 % of cats over 15 years of age show CKD sign (Bartlett et al., 2010).

Because of the fact that repair of kidney injury is incomplete, episodes of kidney injury lead to the CKD (Kramann et al., 2015). Therefore, understanding of the pathogenesis of CKD development could provide an efficient approach for alleviating the high morbidity and mortality accompanied the CKD, and also meet up the objective of 'Zoobiquity'. There are many causes of CKD, including hypertension, diabetes, certain infections, long-term drug use, and systemic disorder such systemic lupus erythematosus (SLE) (Lysaght, 2002; Kriz and LeHIr, 2005; Nakai et al., 2006; Smyth et al., 2014). Irrespective of etiologies, CKD is resulted from damage to the blood-urine barrier (BUB) components (Ohashi et al., 2002; Kimura et al., 2013).

In glomerulus, BUB is formed by inner endothelium, middle glomerular basement membrane (GBM) and outer podocyte (Satchell and Braet, 2009). Glomerular capillary

endothelium plays critical coordinating roles in renal physiology (Endemann and Schiffrin, 2004; Cheng et al., 2014). However, it has been reported that development of glomerulosclerosis in murine model resulted from an imbalance in the decrease in endothelial repair and increase in endothelial apoptosis after renal injury (Tang et al., 2014). Furthermore, the podocyte is involved in the maintenance of healthy intracapillary environments through crosstalk with glomerular endothelial cells (ECs) and as a source of vascular endothelial growth factor (VEGF) in glomeruli (Nihalani and Susztak, 2013; Kobayashi et al., 2015). Recently it has been revealed that podocyte injury is a critical event that causes albumin hyperfiltration from glomerular capillaries and causes glomerulonephritis (GN) in mice (Kimura et al., 2013). Therefore, when this BUB is not functioning properly, it ceases to be an effective barrier and leads to proteinuria and CKD.

Similarly, renal tubular epithelial cells (TECs) and ECs of peritubular capillary (PTC) have important role for the barrier between renal tissues and blood stream, by reabsorption of filtrate components into PTC and trafficking of leukocytes from blood stream to extravascular space, respectively (Khakpour et al., 2015; Vedulla et al., 2017). However, PTC ECs show differential responses to microenvironmental changes or stimuli. They are also injured in different nephropathy, resulting in a reduction in capillary density and progression of tubulointerstitial lesions (TILs) (Lindenmeyer et al., 2007). In some disease, inflammatory cells infiltrate to tubulointerstitium caused PTC injury (Ohashi et al., 2002). Importantly, PTC rarefaction, along with interstitial fibrosis and tubular atrophy, is one of the major hallmarks of CKD (Kida et al., 2014). Interestingly, TECs undergo a morphological changes in response to variety of injury and function as inflammatory and fibrogenic cells (Liu et al., 2018). These data indicate that injury of BUB components in tubulointerstitium also causes kidney disease.

Moreover, BUB components, including ECs, podocytes and TECs are recognized as active participants in the host's innate immune response to infection and injury. They express toll-like receptors (TLRs) which are activated by different stimuli. Endogenous TLR ligands may act as danger signals relaying the presence of tissue injury to immune cells or BUB component cells, thereby inducing inflammation and damage of local tissue (Anders et al., 2003; Baccala et al., 2009; Garraud and Cognasse, 2010; Salvador et al., 2016; Xia et al., 2017). Taken together, these studies strongly suggest that understanding the pathological crosstalk between components of BUB and their achieved immunological function is invaluable for the development of better diagnostic and therapeutic strategies for CKD.

Therefore, the author focused importance on endothelium and other components of BUB to clarify pathophysiological and immunological role of BUB in the progression of kidney disease in model mice. In Chapter 1, the author showed the pathological crosstalk between components of glomerular BUB, including ECs and podocytes using a modified scanning electron microscopy (mSEM) in addition to routine histopathological techniques. In Chapter 2, the author revealed the pathological interaction between components of tubulointerstitital BUB, including PTC ECs and TECs. In third Chapter, the author showed overexpression of *Tlr9* in different components of BUB in glomerulus and tububulointerstitium of autoimmune GN (AGN) model mice. In addition, the author investigated the activation of different BUB components through overexpression of *Tlr9* and subsequent development of GLs and TILs in AGN model mice.

In conclusion, the integrity of BUB depends on the plasticity and dynamic signaling between its components, and the author also considered TLR9 as a novel theranostic target for the treatment of AGN.

Contents of this research were published in the following articles

1. Masum, M.A., Ichii, O., Elewa, Y.H.A., Nakamura, T., and Kon, Y. 2017. Local CD34-positive capillaries decrease in mouse models of kidney disease associating with the severity of glomerular and tubulointerstitial lesions. *BMC Nephrol.*, **18**: 280.

2. Masum, M.A., Ichii, O., Elewa, Y.H.A., Nakamura, T., Otani, Y., Hosotani, M., and Kon, Y. 2018. Modified scanning electron microscopy reveals pathological crosstalk between endothelial cells and podocytes in a murine model of membranoproliferative glomerulonephritis. *Sci. Rep.*, **8**: 10276.

3. Masum, M.A., Ichii, O., Elewa, Y.H.A., Nakamura, T., Otani, Y., Hosotani, M., and Kon, Y. 2018. Overexpression of Toll-like receptor 9 correlates with podocyte injury in a murine model of autoimmune membranoproliferative glomerulonephritis. *Autoimmunity*, DOI: 10.1080/08916934.2018.1549234.

Chapter 1

Modified scanning electron microscopy revealed pathological crosstalk between components of glomerular blood-urine barrier

Introduction

Kidney disease causes a systemic deterioration in health. The CKD, in particular, is a substantial public health burden because it is associated with ESRD and cardiovascular disease (Tonelli et al., 2006). There are many causes of CKD, including hypertension, diabetes, certain infections, long-term drug use, and systemic disorder such as SLE (Lysaght, 2002; Kriz and LeHIr, 2005; Nakai et al., 2006; Smyth et al., 2014). Importantly, GN is considered as the second most cause of renal failure (Segelmark and Helmark, 2010).

The adult kidney filters blood to eliminate toxins and metabolic wastes, maintains the balance of water, salts, and pH, absorbs minerals, produces urine, etc., to sustain life. The glomerular BUB plays key roles to execute these functions. Defects in BUB integrity were observed during the progression of GN with leakage of plasma proteins, including albumin, finally leading to ESRD (Kimura et al., 2013). The occurrence of proteinuria was associated with podocytopathy and decreased podocyte number in AGN (Kimura et al., 2013). Interestingly, it has been reported that, in healthy individuals, podocytes produced VEGF which was essential for maintenance of adjacent endothelia and integrity of its fenestration (Kobayashi et al., 2015; Scott and Quaggin, 2015). Additionally, it has been reported that the glomerular endothelium was covered with a glycocalyx forming a permeability barrier preventing the development of proteinuria under normal healthy conditions (Abras et al., 2006; Satchell and Braet, 2009). Therefore, pathologies of ECs and their fenestration are associated with proteinuria and renal failure, which have been well characterized in preeclampsia and diabetes (Stillman and Karumanchi, 2007; Toyoda et al., 2007; Weil et al., 2012). Moreover, an interaction between the endothelium and podocytes through VEGF has been reported in diabetes (Sivaskandarajah et al., 2012).

Furthermore, Haraldson *et al*. have reported that the BUB function was considered an integrated whole with cell-cell interaction, and any disruption of such interaction could affect the overall permeability (Haraldson et al., 2008). However, limited information is available regarding the defective interactions between podocytes and glomerular endothelium during CKD pathogenesis, including AGN revealed by combined ultrastructural and molecular approaches.

For the ultrastructural analysis of the glomerulus, scanning electron microscopy (SEM) and transmission electron microscopy (TEM) are useful. However, the ultrastructural quantitative analysis of the glomerulus, including enumeration of endothelial fenestrations (EFs) and podocyte foot process (PFP), is quite difficult, because SEM reveals only the surface of glomerular ECs or podocytes, and the area is limited for TEM observation. Interestingly, Koga *et al*. have performed SEM using a semi-thin section and reported that this method could aid visualising large areas of sections and obtain TEM-like images (Koga et al., 2015). Therefore, in this study, the author modified the previous SEM method to develop the so-called "mSEM" and applied this method for the analysis of glomerular ultrastructural pathology, especially focusing on AGN.

In this study, the author used BXSB/MpJ-*Yaa* (Yaa) mice as a murine model of AGN. Mice of this strain develop systemic autoimmune disease characterised by increased serum autoantibody titres, autoreactive B cells, vasculitis, and podocyte injury with AGN (Kimura et al., 2013). Yaa mice carries a genetic mutation on the Y chromosome called "Y-linked autoimmune acceleration" (*Yaa)*, and male mice develop more severe GN than female mice due to the *Yaa* mutation (Santiago-Raber et al., 2004).

In Chapter 1, the author clearly revealed pathological correlations between the glomerular BUB components, including endothelial and podocyte injury in AGN

pathogenesis through a unique ultrastructural analysis and molecular quantitative analysis.

Materials and Methods

Ethical statements

All animal experiments were approved by the Institutional Animal Care and Use Committee of the Faculty of Veterinary Medicine, Hokkaido University (approval No. 13-0032, 15-0079). The authors adhered to approved Guide for the Care and Use of Laboratory Animals of Hokkaido University, Faculty of Veterinary Medicine (approved by the Association for Assessment and Accreditation of Laboratory Animal Care International).

Experimental animal and housing

Male BXSB/MpJ (BXSB), a wild-type strain, and Yaa mice were purchased from Japan SLC Inc. (Hamamatsu, Japan). Yaa mice were used as autoimmune AGN model mice and age-matched BXSB mice served as the healthy control. All mice were maintained in specific pathogen-free conditions in a 1:1 light-dark condition. Food and water were provided *ad libitum* to experimental mice.

Sample preparation

Mice were deeply anaesthetised with a mixture of 0.3 mg/kg medetomidine (Kyoritsu Seiyaku, Tokyo, Japan), 4 mg/kg midazolam (Astellas Pharma, Tokyo, Japan), and 5 mg/kg butorphanol (Meiji Seika Pharma, Tokyo, Japan), and urine was collected through urinary bladder puncture. Mice were euthanized by exsanguination from femoral artery. Blood and kidneys were collected for serological and histopathological analysis, respectively.

The harvested kidneys were cut into small slices and fixed with 10% neutral buffered

formalin (NBF), 4% paraformaldehyde (PFA), or 2.5% glutaraldehyde (GTA) in 0.1 M phosphate buffer (PB) for histopathological analysis, immunofluorescence staining, and ultrastructural analysis, respectively.

Serum and urine analysis

Serum levels of anti-dsDNA antibody in all mice were measured using Mouse Anti-dsDNA Ig's (Total A+G+M) ELISA kit (Alpha Diagnostic International, San Antonio, TX, USA) to evaluate the autoimmune condition. Serum levels of blood urea nitrogen (sBUN) and creatinine (sCr) in all mice were measured using Fuji Drichem 7000v (Fujifilm, Tokyo, Japan) to examine kidney function. Urinary albumin-to-creatinine ratio (uACR) was determined using Albuwell M and Creatinine Companion kits (Exocell, Philadelphia, PA, USA).

Histopathological examination

Paraffin embedded blocks of kidney specimens fixed with NBF were cut at a thickness of 2 μm and stained with periodic acid Schiff-hematoxylin (PAS-H) and periodic acid methenamine silver (PAM) to examine histopathology of the glomerulus. Immunodetection of cell markers for B cells (B220), T cells (CD3), capillary ECs (CD34), macrophages (Iba1), podocytes [Nephrin, Podocin, Synaptopodin, and Wilms tumor1 (WT1)], and VEGF A was performed. Staining conditions are listed in Table 1-1. Briefly, deparaffinised kidney sections were subjected to antigen retrieval. Thereafter, the slides were submerged in methanol containing 3% H_2O_2 for 20 min at 25°C and blocked with normal goat or donkey serum. Sections were incubated with primary antibody overnight at 4°C. After washing in phosphate-buffered saline (PBS), the sections were incubated

with respective biotinylated or Alexa Fluor 488-labelled secondary antibodies (Table 1-1) at 25°C for 30 min and then washed with PBS. For immunofluorescence, the tissue sections were incubated with Hoechst 33342 (1: 200; Dojingo, Kumamoto, Japan) for nuclear staining at room temperature for 5 min and examined under All-in-One Fluorescence Microscope BZ-X710 (Keyence, Osaka, Japan). For immunohistochemistry, the sections were incubated with biotinylated secondary antibody and then streptavidin-horseradish peroxidase (SABPO kit; Nichirei, Tokyo, Japan) for 30 min followed by incubation with 3,3-diaminobenzidine tetrahydrochloride-H_2O_2 solution. Finally, the sections were counterstained with hematoxylin and dehydrated with ascending grades of alcohols.

Electron microscopy

The author modified the method described by Koga *et al*. to obtain TEM-like images using SEM (mSEM, Fig. 1-1) (Koga et al., 2015). Briefly, small pieces of kidney sections were fixed with 2.5% GTA in 0.1 M PB for 4 h at 4°C followed by post-fixation with 1% osmium tetroxide (OsO_4) in 0.1 M PB for 2 h. Then, specimens were dehydrated with ascending grades of alcohol and embedded in epoxy resin (Quetol 812 Mixture; Nisshin EM, Tokyo, Japan). The Epon blocks were cut at a thickness of 500 nm. Semi-thin sections were mounted on cover glass slides and incubated at 60°C for 30 min after staining with toluidine blue. The sections were stained with uranyl acetate and lead citrate for 20 min and 15 min, respectively. The section containing cover glass was mounted on the specimen stub using two-sided adhesive and sputter-coated for 60 s with Hitachi E-1030 ion sputter coater (Hitachi, Tokyo, Japan), and then examined using an S-4100 SEM (Hitachi) with an accelerating voltage of 4 kV.

For routine SEM, small pieces of GTA-fixed kidney were treated with tannic acid and post-fixed with 1% OsO_4 for 1 h. The specimens were dehydrated with grades of alcohol, transferred into 3-methylbutyl acetate, and finally dried with HCP-2 critical point dryer (Hitachi). The specimens were then examined with an S-4100 SEM. For TEM examination, small pieces of kidney were pre-fixed with 2.5% GTA in 0.1 M PB for 4–6 h at 4°C and post-fixed with 1% OsO_4 in 0.1 M PB for 2 h at 4°C, and then dehydrated in grades of alcohol and embedded in epoxy resin. Ultrathin sections were cut at 60 nm and stained with uranyl acetate and lead citrate. The specimens were observed under a TEM (JEM-1210; JEOL, Tokyo, Japan).

Histoplanimetry

Digital images of more than 40 randomly selected glomeruli from each mouse were obtained at 400× magnification using BZ-X710 (Keyence) for all examined parameters. The size and number of total cells in each glomerulus were determined using PAS-H-stained sections. The number of B220^{+} B cells, CD3^{+} T cells, Iba1^{+} macrophages, WT1^{+} podocytes, and the immunopositive area for CD34^{+} capillaries and that for Nephrin^{+}, Podocin^{+}, or Synaptopdin^{+} reactions in the digital images of glomeruli were measured using immunofluorescence sections and a BZ-X Analyzer (Keyence). Images of 50 capillaries and their adjacent podocyte were obtained using mSEM examination and analysed using ImageJ (National Institute of Health, Bethesda, MD, USA) software to count EF and PFP per micrometre of length.

Statistical analysis

The results were expressed as the mean ± standard error. For comparisons between healthy controls and diseased mice, a nonparametric Mann–Whitney U test ($P < 0.05$) was utilized. The Kruskal-Wallis's test was used to compare between groups, and multiple comparisons were performed using Scheffe's method when significant differences were observed ($P < 0.05$). The correlation between two parameters was analysed using Pearson's rank correlation test ($P < 0.01$).

Results

Pathology of the AGN model

Glomerular histopathology was examined in kidney sections from Yaa mice and their respective control BXSB mice at 3, 4, and 6 months of age (Fig. 1-2). In BXSB mice, no GLs were observed in all ages examined (Fig. 1-2A-C). However, Yaa mice showed specific lesion development depending on age. Yaa mice at 3 months of age did not show any lesions, but some of them developed mild GN at 4 months of age (Fig. 1-2D and E). Yaa mice at 6 months of age clearly developed AGN characterised by glomerular hypertrophy, increased glomerular cell number, and PAS-H-positive material depositions in the mesangial area (Fig. 1-2F). There was no thickening of GBM in all ages of BXSB glomerulus (Fig. 1-2G-I) and in Yaa mice at 3 months of age (Fig. 1-2J). Though mild GBM thickening was observed in Yaa mice glomerulus at 4 months of age (Fig. 1-2k), it was more thickened and wrinkled in 6-month-old Yaa mice (Fig. 1-2L).

Other histopathological and clinical parameters were estimated at 6 months of age as Yaa mice showed clear lesions at this age. Yaa mice at 6 months of age displayed significantly higher values in glomerular size and cell number, an index for systemic autoimmune abnormality (anti-dsDNA antibody level), and renal functional indices (uACR, sBUN and sCr) (Table 1-2). These data indicate the development of AGN in Yaa mice at 6 months of age. Immunohistochemistry for B220, CD3, and Iba1 to detect B cells, T cells, and macrophages, respectively, revealed that they were present in the glomerulus of Yaa mice at 6 months of age compared with BXSB mice (Fig. 1-3A-F), and these quantitative results were significantly higher in the former than in BXSB mice (Fig. 1-3G).

Loss of glomerular EF with podocyte injury examined through mSEM method in the

AGN model

The author modified and applied the previously described method for quantitative analysis of EF and PFP, and this was the first attempt at applying mSEM for pathological analysis (Fig. 1-4). Firstly, the author could examine the same area of normal glomerulus in 6 months-old BXSB mice using light microscopy (Fig. 1-4A), TEM (Fig. 1-4B-D), and mSEM (Fig. 1-4E-G). EFs and PFPs were clearly observed through both TEM (Fig. 1-4C and D) and mSEM (Fig. 1-4F and G). Furthermore, the author also examined the glomerulus of 6 months-old Yaa mice (Fig. 1-4H-N). EC hypertrophy with loss of EF and thickened GBM with electron-dense deposits was clearly visible in Yaa mice using both TEM (Fig. 1-4I-K) and mSEM (Fig. 1-4L-N), indicating the usefulness of mSEM to examine the glomerular ultrastructure, similar to TEM.

Figure 1-5 shows the ultrastructural features of EF and PFP using mSEM and SEM. mSEM in BXSB mice revealed that EFs and PFPs clearly lined the GBM in all ages examined (Fig. 1-5A and B). Yaa mice showed normal endothelium with fenestrations at 4 months of age, but slight PFP effacement was also observed at this stage (Fig. 1-5C). However, in Yaa mice at 6 months of age, thickened GBM with electron-dense deposits was lined by hypertrophied ECs with loss of EF and injured podocytes with PFP effacement (Fig. 1-5D). This is consistent with the results obtained using SEM, wherein BXSB glomerular capillary endothelium contained numerous EFs and normal PFPs at all stages (Fig. 1-5E and F). However, Yaa mice showed normal glomerular EFs and loss of EFs at 4 and 6 months of age, respectively (Fig. 1-5G and H). BXSB mice showed normal PFPs at all examined stages (Fig. 1-5I and J), but Yaa mice at 4 months of age showed microvillus-like structure protruding from podocytes and mild PFP effacement (Fig. 1-

5K). Numerous microvillus-like structures and PFPs effacement was observed in Yaa mice at 6 months of age (Fig. 1-5L). Quantification analysis using mSEM showed that the number of EFs and PFPs significantly decreased in Yaa mice compared with BXSB mice (Fig. 1-5M) at 6 months of age.

Downregulation of glomerular capillary endothelium marker, podocyte functional molecules, podocytes, and VEGF A in the glomerulus of the MPGN model

The author next examined the expression of the capillary endothelium marker (CD34) and podocyte functional molecules (Nephrin, Podocin, and Synaptopodin) in the glomerulus of BXSB and Yaa mice (Fig. 1-6A-L). CD34$^+$ reactions were detected in the glomerular and PTC in the BXSB kidney using immunofluorescence staining (Fig. 1-6A and B, E and F, and I and J). Yaa mice at 4 months of age also showed normal CD34$^+$ expression (Fig. 1-6C, G, and K); however, glomerular capillaries were faint in the Yaa glomerulus at 6 months of age (Fig. 1-6D, H, and L). Furthermore, linier positive reactions for podocyte functional molecules (Nephrin, Podocin, and Synaptopodin) were clearly observed along with the glomerular capillary rete in BXSB mice at 4 and 6 months of age (Fig. 1-6 A, B, E, F, I, and J). Podocyte functional molecules expression tended to be faint at the centre of glomerulus in the 4-month-old Yaa glomerulus (Fig. 1-6C, G and K), but they were faint and tended to be localised only at the peripheral area in the Yaa glomerulus at 6 months of age (Fig. 1-6 D, H and L). Importantly, podocyte function molecules were retained in those areas where CD34$^+$ capillaries existed in Yaa mice. For quantification analysis, the immunopositive areas for Nephrin, Podocin, and Synaptopodin were decreased in 4- month-old Yaa mice compared to in BXSB mice. However, the immunopositive areas for CD34, Nephrin, Podocin, and Synaptopodin in

16

the glomerulus were significantly decreased in Yaa mice at 6 months of age (Fig. 1-6M).

WT1[+] podocytes were uniformly distributed throughout the BXSB glomerulus at 4 and 6 months of age (Fig. 1-7Aand B). Yaa mice at 4 months of age showed decreasing tendency for WT1^{+} podocytes (Fig. 1-7C); however, few podocytes were retained in Yaa mice at 6 months of age (Fig. 1-7D). The number of podocytes also significantly decreased in the glomerulus of Yaa mice compared to in BXSB mice at 4 and 6 months of age (Fig. 1-7E). VEGF A produced by podocytes in the glomerulus is responsible for the maintenance of the adjacent endothelium (Breier et al., 1992). The author observed a VEGF A positive reaction in the glomerulus of BXSB mice at all stages (Fig. 1-7F and G). However, weakly positive results were observed in Yaa mice at 4 and 6 months of age (Fig. 1-7H and I). The immunopositive area of VEGF A also significantly decreased in the glomerulus of Yaa mice compared to in BXSB mice at 4 and 6 months of age (Fig. 1-7J).

Pathological correlation between histopathological and clinical parameters

The author examined the statistical correlations of histoplanimetric values including glomerular EC injury (CD34^{+} area and EF number), podocyte injury (positive area for Nephrin, Podocin, Synaptopodin, and WT1, and PFP number), VEGF A^{+} area, glomerular damage indices (glomerular size and cell number), infiltrating immune cells (B cell, T cell, and macrophage), and clinical parameters (sBUN, sCr, uACR, and serum anti-dsDNA antibody level) at 6 months of age (Table 1-3). The CD34^{+} area and EF were significantly and positively correlated with all examined values, except for sCr. PFP and VEGF A^{+} areas were also significantly and positively correlated with all examined values, except for sCr (Table 1-3).

Discussion

Yaa mice at 4 months of age showed individual discrepancy in the development of lesions, and some of them showed mild GN characterised by injury of podocytes, but no abnormalities in endothelium. AGN were clearly observed in 6-month-old Yaa mice. In this study, the author showed a series of pathological crosstalk between endothelium and podocytes in different ages of AGN model mice, using mSEM to monitor the progression of this disease.

TEM is usually used for ultrastructural analysis in both basic and clinical studies. However, TEM sample preparation and ultra-thin sectioning are complex and time-consuming. Moreover, TEM can examine only a small observation area, and this makes the quantitative ultrastructure study more laborious and prolonged. Therefore, the author modified the previously described SEM method (Koga et al., 2015) and demonstrated its efficacy for renal pathological analysis for the first time. In healthy BXSB mice, glomerular EF and PFP were clearly observed using both TEM and mSEM. Moreover, in Yaa mice, clear GLs such as endothelial thickening with decreased EF, loss of podocyte at the center of the glomerulus, GBM widening, immune-complex (IC) depositions in GBM, and PFP effacement were detected using both TEM and mSEM. Therefore, mSEM is an effective method to evaluate the glomerular ultrastructure in both basic and clinical studies.

The combinations of mSEM and immunostaining methods revealed that Yaa mice had endothelial injury with EF loss and decreased CD34^{+} area in the glomerulus. Glomerular capillary endothelium is highly flattened, fenestrated, and has glycocalyx covering the luminal surface, essential for formation of glomerular ultrafiltrate and permeability barrier (Ballermann, 2005; Haraldsson et al., 2008; Curry and Adamson, 2012). Therefore,

EC injury with morphological alternations is crucial for the development of GLs and TILs in the kidney (Ohashi et al., 2000; Kang et al., 2002). In this study, EF number and CD34^{+} area decreased and was strongly correlated with the indices for glomerular damage and renal dysfunction. The author considered autoimmune disease-mediated inflammation as a key factor for the pathogenesis of endothelial injuries, because of the presence of glomerular inflammatory cells including B cells, T cells, and macrophages. A previous study reported that B cells could play a role in antibody production, activation of pathogenic T cells, and secretion of pro-inflammatory cytokines including tumor necrosis factor (TNF) and interleukin (IL-6), all of which contribute to GLs in lupus-prone mice (Chan et al., 1999; Bekar et al., 2010). Moreover, macrophages and their products resulted in cytotoxicity, basement membrane damage, decreased glomerular filtration rate, mesangial cell proliferation, and glomerulosclerosis (Nikolic-Paterson and Atkins, 2001). Therefore, the author considered that B cells could play roles not only in antibody production, but also in the activation of T cells and macrophages, which might cause GN through endothelial injury.

mSEM revealed loss of podocyte, PFP effacement at 4 and 6 months of age. Similarly, the immunopositive area for podocyte functional molecules was decreased at 4 and 6 months. These data indicate that mSEM is useful for analysing the glomerular ultrastructure in the disease state. Podocytes are specialized perivascular cells that maintain the BUB through formation of podocyte functional molecules and interaction with adjacent endothelium (Frey and Olson, 2003; Saleem et al., 2002; Scott and Quaggin, 2015; Nagata, 2016). The impaired expression of podocyte functional molecules is a primary contributor to the development of podocyte injury and subsequent albuminuria in several glomerular diseases including glomerular sclerosis (Kriz et al., 1998; Orikasa

et al., 1998; Roselli et al., 2004; Yi et al., 2007; D'Agati et al., 2011; Unnersio-Jess et al., 2016). Pro-inflammatory cytokines, including TNF and IL-6, and activated T cells cause loss of podocyte functional molecule proteins, and disarrangement of the actin cytoskeleton results in PFP effacement (Kimura et al., 2013).

Interestingly, Toyoda *et al*. have reported that podocyte detachment and reduced glomerular EF were related to classical diabetic nephropathy lesion (Toyoda et al., 2007). Similar to this report, in this Chapter, podocyte diaphragm molecules remained in those areas where CD34$^+$ capillary existed, and podocyte injury indices were strongly correlated with glomerular capillary injury in Yaa mice. Moreover, other studies have showed imbalanced production of endothelial nitric oxide, activated protein C, and endothelin type 1 receptor from glomerular endothelium-mediated podocyte injury in GN (Isermann et al., 2007; Daehn et al., 2014). These results strongly suggest the functional correlation between glomerular endothelium and podocytes.

The fenestrated endothelium is usually located adjacent to epithelial cells that express high levels of VEGF, and the highest level of VEGF mRNA was found in mature glomerular podocytes (Breier et al., 1992). Furthermore, the formation of glomerular capillary EF critically depends on VEGF A from differentiated podocytes (Breier et al., 1992). Eremina *et al*. have reported that podocyte-specific deletion of a single allele of VEGF A resulted in loss of endothelial differentiation without any fenestration (Eremina et al., 2003). Interestingly, VEGF signalling was not involved in the endothelial-podocyte interaction until advanced podocyte injury was established (Daehn et al., 2014). In this Chapter, the author showed uniform expression of VEGF A at all ages of BXSB mice. VEGF A$^+$ area began to decrease in 4-month-old Yaa mice glomerulus, but was drastically reduced at 6 months. Furthermore, the VEGF A$^+$ area was strongly correlated with

podocyte and glomerular endothelial injury only at 6 months. Therefore, a severely injured and/or reduced number of podocytes produced a lower quantity of VEGF A. This decreased the bioavailability of VEGF A in the glomerulus, resulting in glomerular endothelial injury and EF loss.

The BUB is a highly complex biological structure maintained by various physiochemical molecules and signalling pathways among its three core components (Menon et al., 2012). The author summarized pathological events in BUB occurring in the AGN model in Fig. 1-8. ECs are dependent on podocytes for VEGF A to maintain their morphology and fenestration. However, inflammatory cells cause podocyte injury resulting in PFP effacement, downregulation of podocyte function molecules, and even loss of whole podocytes. This injury and loss of podocytes causes proteinuria. Moreover, loss of podocyte at the center of the glomerulus lead to glomerulosclerosis at that area. Simultaneously, VEGF A production drastically reduced from the severely injured podocytes, which aggravates endothelial damage resulting in loss of fenestration. In addition, imbalanced production of signalling molecules from injured endothelium also affects podocytes. Hence, glomerular capillary endothelial and podocyte injury mutually disrupts BUB components and leads to AGN pathogenesis. Therefore, the author looked forward to clarify tubulointerstitial BUB in next Chapter.

Summary

In Chapter 1, the author evaluated crosstalk between ECs and podocytes, components of the glomerular BUB, in the progression of AGN using mSEM analysis as well as other molecular techniques.

Yaa mice exhibited AGN characterised by elevated serum autoantibody levels, albuminuria, renal dysfunctional parameters, and decreased EF and PFP effacement with immune cell infiltration. Similar to TEM, mSEM revealed a series of pathological changes in GBM and densities of EF and PFP in Yaa compared with control BXSB at different stages. Further, immunopositive area of endothelial marker (CD34), podocyte functional molecules (Nephrin, Podocin, Synaptopodin, and WT1), and VEGF A significantly decreased in the glomerulus of Yaa compared with BXSB at final stage. The indices of glomerular endothelial injuries and podocyte injuries were also significantly correlated with each other and with indices of autoimmune disease and renal dysfunction.

Thus, the author elucidated the pathological crosstalk between ECs and podocytes in AGN progression and the usefulness of mSEM for glomerular pathological analysis.

Tables and Figures

Table 1-1: Summary of immunostaining conditions

	B220	CD3	CD34	Iba1	Nephrin	Podocin	Synaptopodin	VEGFA	WT1
Antigen retrieval	CB 105°C, 20 min	TB 105°C, 20 min	CB 105°C, 20 min	0.1% pepsin 37°C, 5 min	CB 105°C, 20 min	CB 105°C, 20 min	TB 105°C, 20 min	CB 105°C, 20 min	CB 105°C, 20 min
Blocking	10% NGS	10% NGS	10% NDS	10% NGS	5% NDS	5% NDS	5% NDS	5% NDS	5% NDS
Primary antibody	Rat polyclonal antibodies (Cedarlane, ON, Canada) 1:1000	Rabbit polyclonal antibodies (Nichirei, Tokyo, Japan) 1:200	Rat polyclonal antibodies (Abcam, Cambridge, UK) 1:400	Rabbit polyclonal antibodies (Wako, Tokyo, Japan) 1:2000	Rabbit polyclonal antibodies (1:500; IBL, Gunma, Japan)	Rabbit polyclonal antibodies (1:800; IBL, Gunma, Japan)	Mouse monoclonal antibodies (1:100; Fitzgerald, MA, USA)	Rabbit polyclonal antibodies (Abcam, Cambridge, UK) 1:200	Rabbit polyclonal antibodies (Santa Cruz, Dallas, TX,USA) 1:150
Secondary antibody	Goat anti-rat IgG (CaltagMedsystems, Buckingham, UK) 1:100 (Biotinylated)	Goat anti-rabbit (SABPO kit, Nichirei, Tokyo, Japan) 1:100 (Biotinylated)	Alexa Fluor 488-labeled donkey anti-rat IgG antibodies (1:500; Life Technologies)	Goat anti-rabbit IgG (SABPO kit, Nichirei, Tokyo, Japan) 1:100 (Biotinylated)	Alexa Fluor 546-labeled donkey anti-rabbit IgG antibodies (1:500; Life Technologies)	Alexa Fluor 546-labeled donkey anti-rabbit IgG antibodies (1:500; Life Technologies)	Alexa Fluor 546-labeled donkey anti-mouse IgG antibodies (1:500; Life Technologies)	Alexa Fluor 546-labeled donkey anti-rabbit IgG antibodies (1:500; Life Technologies)	Alexa Fluor 546-labeled donkey anti-rabbit IgG antibodies (1:500; Life Technologies)

CB: citrate buffer, TB: tris buffer, NGS: normal goat serum and NDS: normal donkey serum

Table 1-2: Glomerular histopathology and clinical parameters

	Glomerular histopathology		Autoimmune indices	Renal function indices		
	Glo. size (µm²)	Glo. cell number	Anti-dsDNA antibody (µg/mL)	uACR (µg/mg)	sCr (µg/dL)	sBUN (µg/dL)
BXSB	3775.75 ± 113.23	34.16 ± 0.98	138.09 ± 21.70	144.93 ±15.52	0.32 ± 0.04	20.60 ± 1.49
Yaa	6241.24 ± 380.69*	72.75 ± 2.44*	712.20 ± 80.95*	801.89 ± 157.85*	0.95 ± 0.26*	74.62 ± 14.13*

Values = mean ± s.e. *: Significant difference from the control group, Mann-Whitney U test (*P < 0.05); N = 4. Glo.: glomerulus, dsDNA : double-strand DNA, uACR: urinary albumin-to-creatinine ratio, sCr: serum creatinine, sBUN: serum blood urea nitrogen, BXSB: BXSB/MpJ and Yaa: BXSB/MpJ-*Yaa.*

Table 1-3. Summary of correlation analysis

Groups	Parameters	CD34+ glomerular capillary		EF number		VEGF A+ glomerular area		PFP number		B cell		T cell		Macrophage	
		ρ	p	ρ	p	ρ	p	ρ	p	ρ	p	ρ	p	ρ	p
ECs	CD34	1.000	-	0.995**	<0.001	0.971**	<0.001	0.986**	<0.001	−0.924**	0.001	−0.979**	<0.001	−0.975**	<0.001
	EF	0.995**	<0.001	1.000	-	0.956**	<0.001	0.981**	<0.001	−0.941**	<0.001	−0.970**	<0.001	−0.981**	<0.001
	VEGF A	0.971**	<0.001	0.956**	<0.001	1.000	-	0.988**	<0.001	−0.904**	0.002	−0.945**	<0.001	−0.963**	<0.001
Podocytes	PFP	0.986**	<0.001	0.981**	<0.001	0.988**	<0.001	1.000	-	−0.929**	0.001	−0.956**	<0.001	−0.976**	<0.001
	Nephrin	0.990**	<0.001	0.991**	<0.001	0.974**	<0.001	0.994**	<0.001	−0.925**	0.001	−0.968**	<0.001	−0.976**	<0.001
	Podocin	0.963**	<0.001	0.973**	<0.001	0.906**	0.002	0.951**	<0.001	−0.918**	0.001	−0.954**	<0.001	−0.959**	<0.001
	Synaptopodin	0.994**	<0.001	0.992**	<0.001	0.974**	<0.001	0.995**	<0.001	−0.928**	0.001	−0.972**	<0.001	−0.978**	<0.001
	WT1	0.997**	<0.001	0.991**	<0.001	0.976**	<0.001	0.986**	<0.001	−0.922**	0.108	−0.970**	<0.001	−0.970**	<0.001
Inflammatory cells	B cell	−0.924**	0.001	−0.941**	<0.001	−0.904**	0.002	−0.929**	0.001	1.000	-	.880**	0.004	−0.976**	<0.001
	T cell	−0.979**	<0.001	−0.970**	<0.001	−0.945**	<0.001	−0.956**	<0.001	0.880**	0.004	1.000	-	−0.949**	<0.001
	Macrophage	−0.975**	<0.001	−0.981**	<0.001	−0.963**	<0.001	−0.976**	<0.001	−0.976**	<0.001	−0.949**	<0.001	1.000	-
Glomerular morphology	Glo. size	−0.920**	0.001	−0.921**	0.001	−0.931**	0.001	−0.932**	0.001	0.943**	<0.001	0.934**	<0.001	−0.959**	<0.001
	Glo. cell	−0.987**	<0.001	−0.982**	<0.001	−0.974**	<0.001	−0.976**	<0.001	0.909**	0.002	0.972**	<0.001	−0.977**	<0.001
Renal function	sBUN	−0.848**	0.008	−0.824*	0.012	−0.795*	0.018	−0.835**	0.010	0.654	0.079	0.818*	0.013	0.724*	0.042
	sCr	−0.690	0.058	−0.700	0.053	−0.664	0.072	−0.689	0.059	0.630	0.094	0.593	0.121	0.696	0.055
	uACR	−0.864**	0.006	−0.835**	0.010	−0.834*	0.010	−0.850**	0.008	0.646	0.083	0.901**	0.002	0.754*	0.031
Autoimmune abnormality	Anti-dsDNA ab	−0.939**	0.001	−0.946**	<0.001	−0.919**	0.001	−0.924**	0.001	0.826*	0.011	0.810**	0.015	−0.762*	0.028

*$P < 0.05$ and **$P < 0.01$, Pearson's rank correlation coefficient; N = 8 (BXSB and Yaa). ECs: endothelial cells; Cap.: capillary, EF: endothelial fenestration, PFP: podocyte foot process, Glo.: glomerulus, sBUN: serum blood urea nitrogen, sCr: serum creatinine, uACR: urinary albumin-to-creatinine ratio, -: not applicable, BXSB: BXSB/MpJ and Yaa: BXSB/MpJ-*Yaa*.
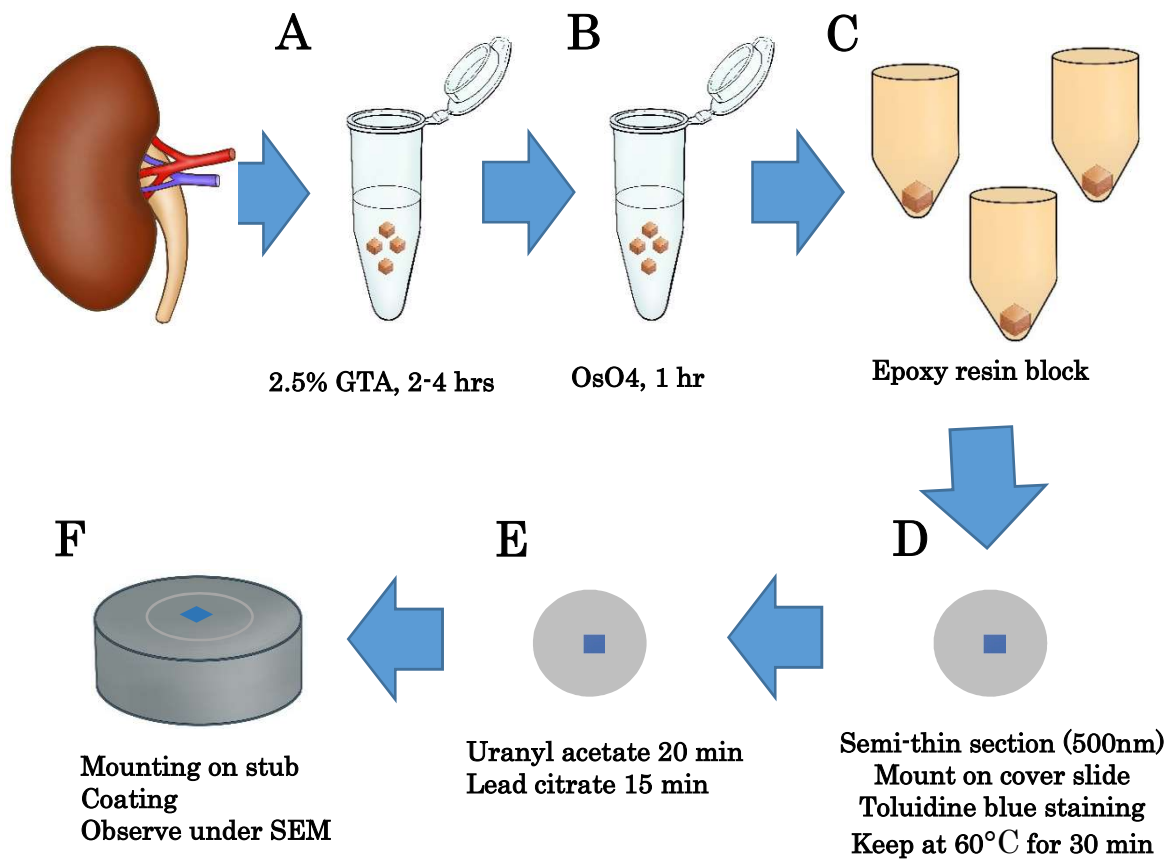
Figure 1-1: Illustration of mSEM method
(a) Fixation of small pieces of kidney with 2.5% GTA for 2-4 hours
(b) Post fixation with 1% OsO_4 for 1 hour.

(c) Embedding in epoxy resin.
(d) Semi-thin sectioning, mounting on cover glass, staining with toluidine blue and drying.
(e) Staining with uranyl acetate and lead citrate.
(f) Mounting on the specimen stub, sputter coating and examination under SEM

GTA: glutaraldehyde, OsO_4: Osmium tetroxide, SEM: scanning electron microscope and mSEM: modified scanning electron microscope.
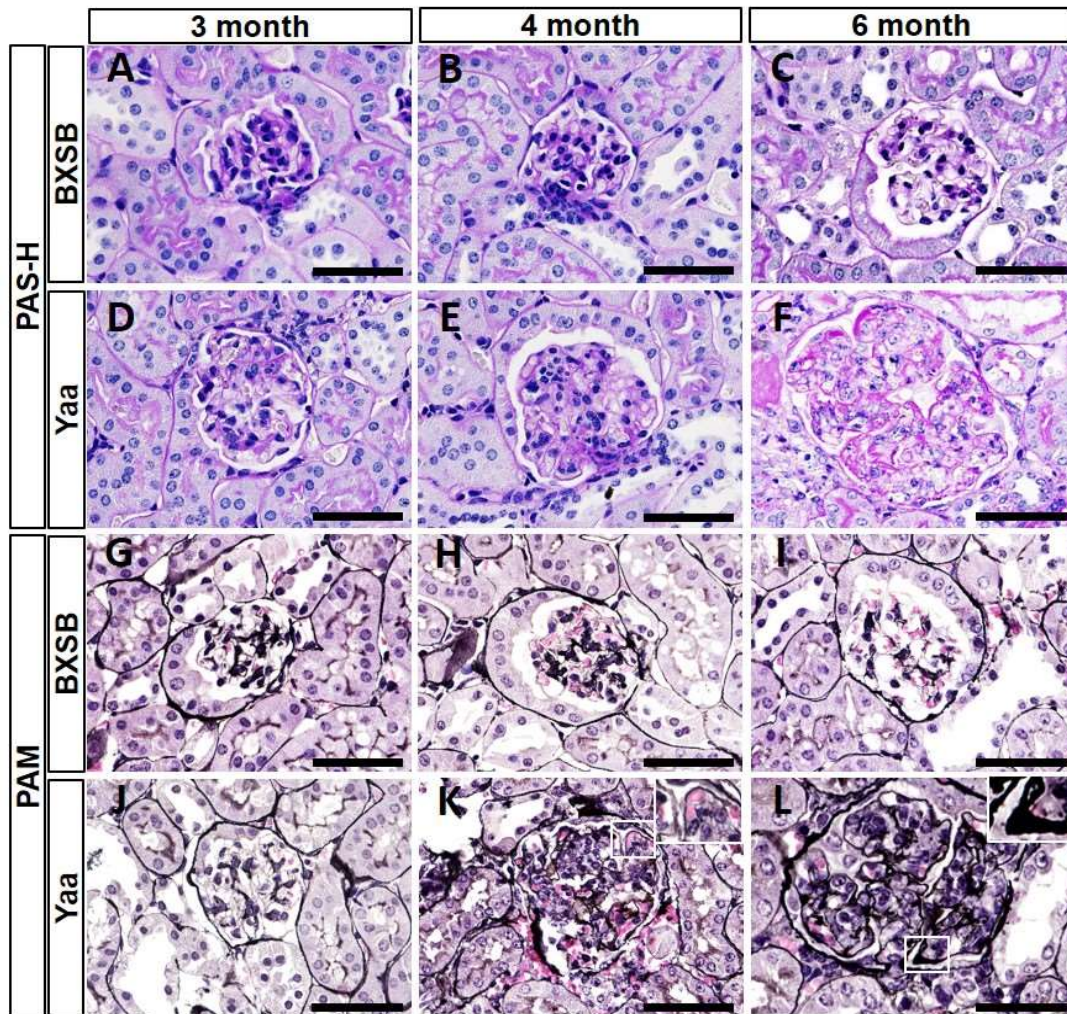
Figure 1-2. AGN in Yaa mice.
(A-F) Glomerular histopathology, PAS-H staining. In BXSB mice, there are no glomerular lesions observed at 3, 4, and 6 months of age (A-C). In Yaa mice, there are no lesions found in glomerulus at 3 months of age (D), but mild glomerulonephritis is found in glomerulus of 4-month-old Yaa mice (E). AGN characterised by increased glomerular size, cell number, and deposition of PAS-H-positive materials is clearly observed in glomerulus of Yaa mice at 6 months of age (F). Bars = 50 μm.
(G-I) Glomerular histopathology, PAM staining. GBM is normal in glomerulus of 3, 4, and 6 month-old BXSB mice (G-I). GBM is normal in glomerulus of 3-month-old Yaa mice (J). Mild glomerular hypertrophy and thickening of GBM is found in Yaa mice at 4 months of age (K). Glomerular hypertrophy, thickening, and wrinkling of GBM are clearly observed in Yaa mice glomerulus at 6 months of age (L). Bars = 50 μm.

BXSB: BXSB/MpJ, Yaa: BXSB/MpJ-*Yaa*, AGN: autoimmune glomerulonephritis, PAS-H: periodic acid Schiff-hematoxylin, PAM: periodic acid methaneamine and GBM: glomerular basement membrane.
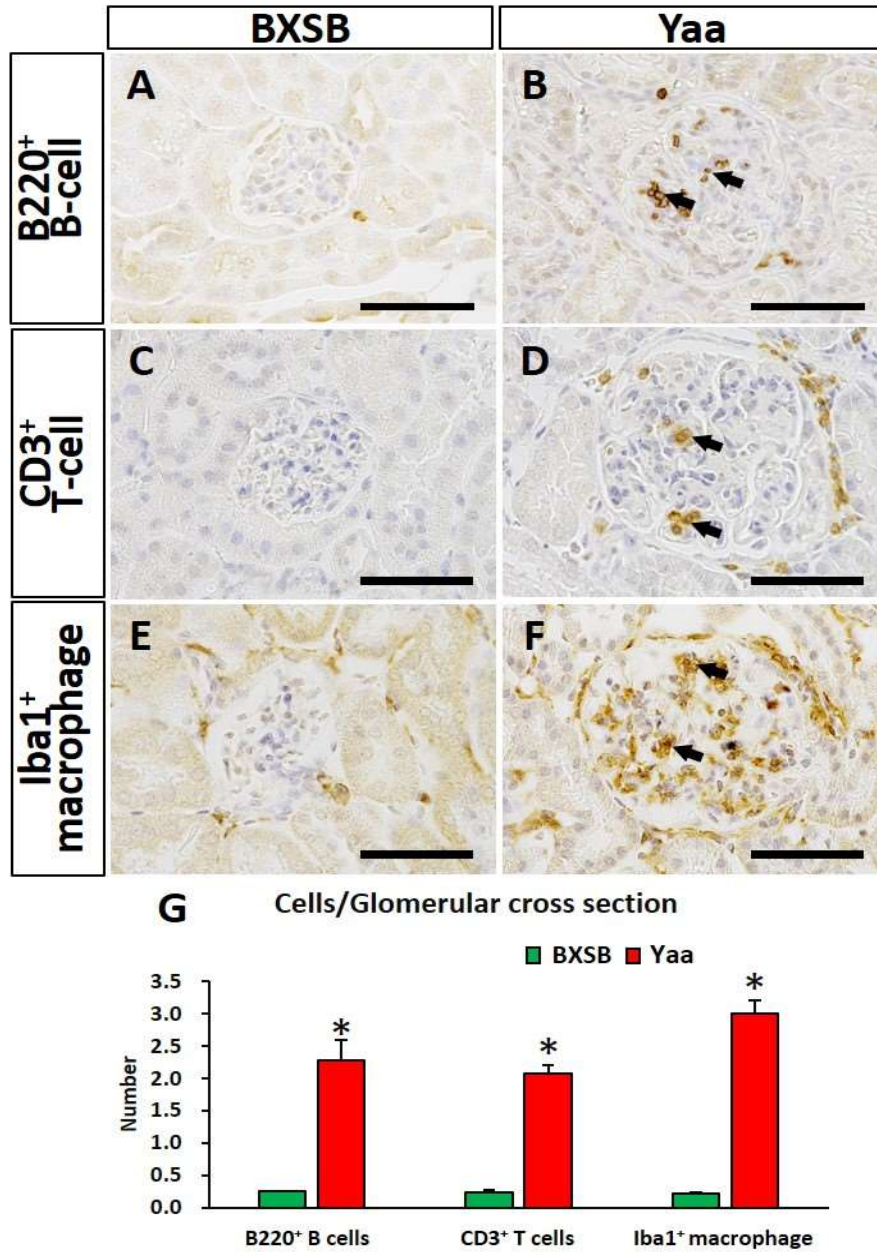
Figure 1-3. **Infiltration of immune cells in the glomerulus.**

(A-F) Infiltration of immune cells in glomerulus, immunohistochemistry. B220^{+} B cells (A and B), CD3^{+} T cells (C and D), and Iba1^{+} macrophages (E and F) are abundant in the glomerulus of Yaa mice (arrows) compared with BXSB mice at 6 months of age. Bars = 50 µm.

(G) Quantification of immune cells in glomerulus of 6-month-old BXSB and Yaa mice. Values = mean ± standard error (s.e.) [*]: Significant difference from the control group, Mann-Whitney *U* test ([*]*P* < 0.05); N = 4.

BXSB: BXSB/MpJ and Yaa: BXSB/MpJ-*Yaa*.

BXSB

A TB

B TEM **C** **D**

E mSEM **F** **G**

Yaa

H TB

I TEM **J** **K**

L mSEM **M** **N**
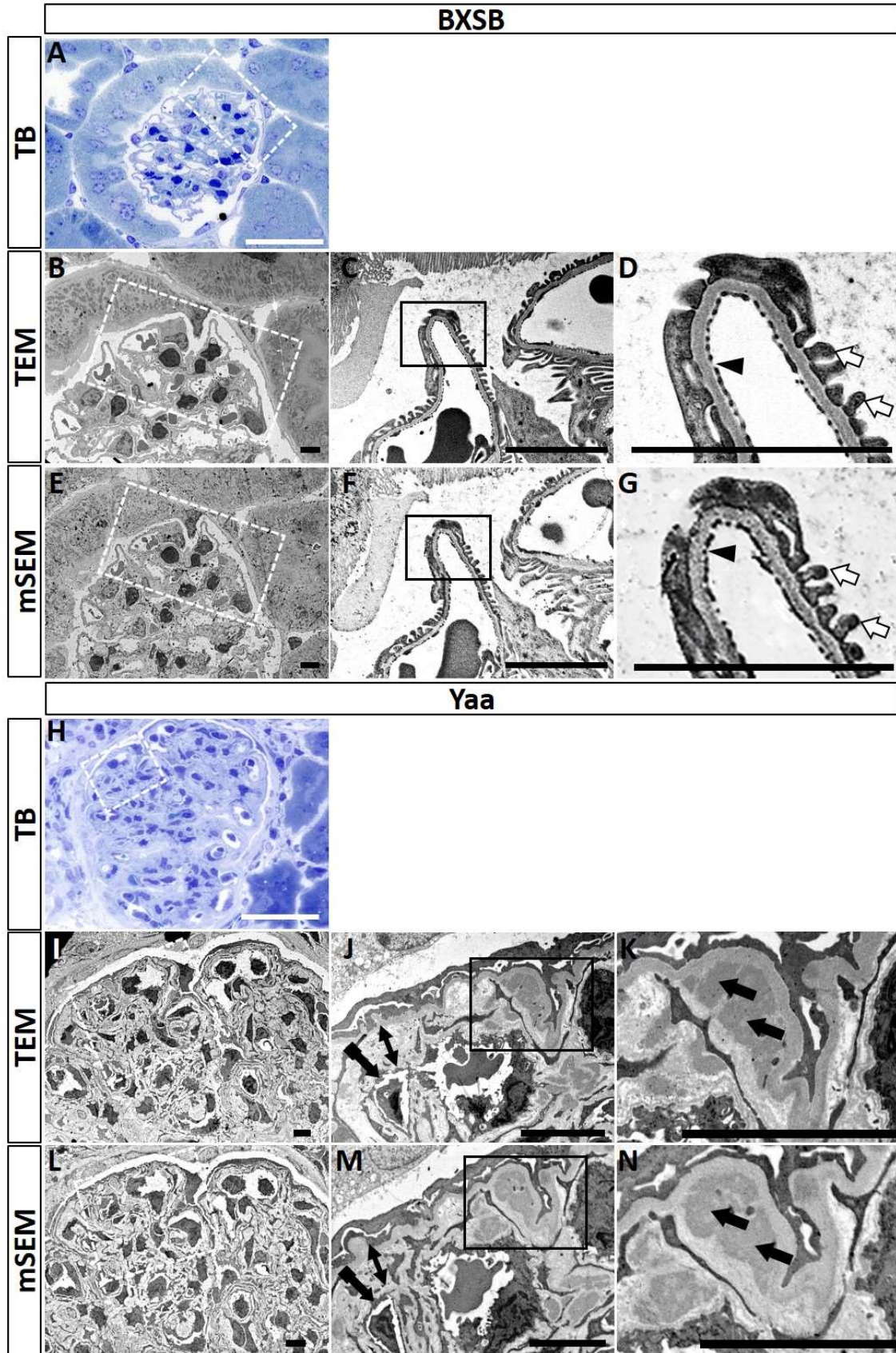
Figure 1-4. Ultrastructures of glomerulus examined by TEM and mSEM in BXSB and Yaa mice at six months of age.

(A) Glomerulus in BXSB mice, TB staining.

(B-D) Glomerulus in BXSB mice, TEM.

(E-G) Glomerulus in BXSB mice, mSEM.

Dashed box area shows same location using different techniques (A, B and E). Normal EF (arrowhead) and PFP (white arrow) are clearly observed using TEM (C and D) and mSEM (F and G). Box area in panels **C** and **F** is magnified in panels **D** and **G**, respectively. Bars = 5 µm.

(H) Glomerulus in *Yaa* mutants, TB staining.

(I-K) Glomerulus in *Yaa* mutants, TEM.

(L-N) Glomerulus in *Yaa* mutants, mSEM.

The dashed area shows the same location using different techniques (H, I and L). GBM widening (two headed arrows), endothelial thickening with loss of EF (tailed arrows), and deposition of electron-dense materials in GBM (black arrows) are clearly visible using both TEM (J and K) and mSEM (M and N). Box area in panels **J** and **M** is magnified in panels **K** and **N**, respectively. Bars = 5 µm.

BXSB: BXSB/MpJ, Yaa: BXSB/MpJ-*Yaa*, TB: toluidine blue, TEM: transmission electron microscopy, mSEM: modified scanning electron microscopy, EF: endothelial fenestration and PFP: podocyte foot process.
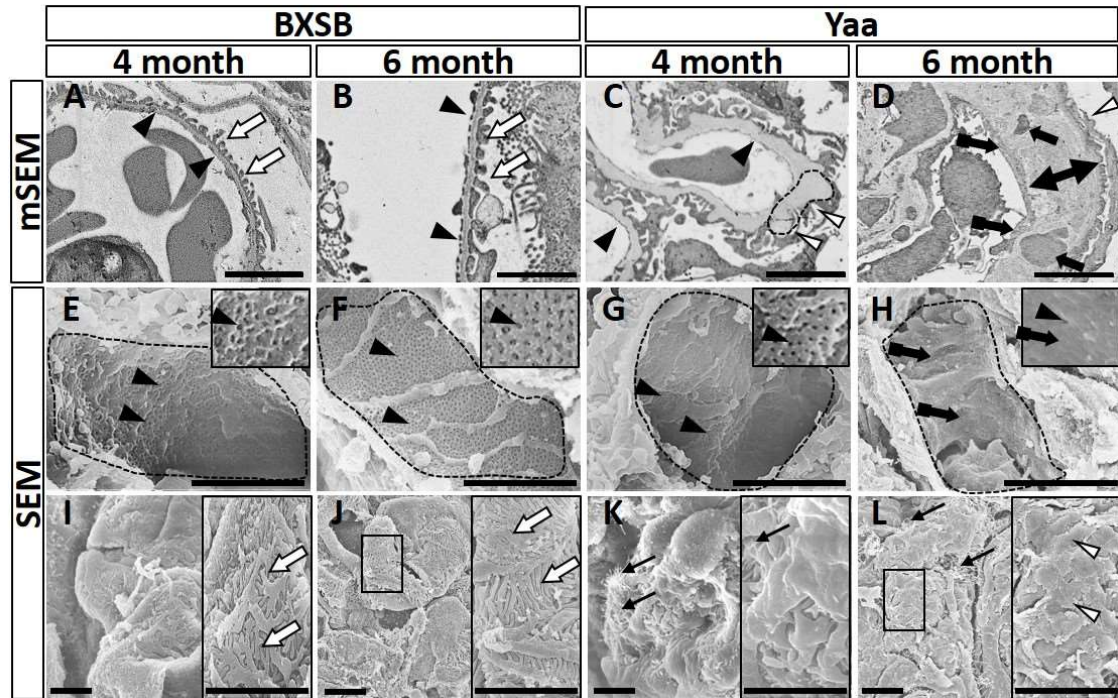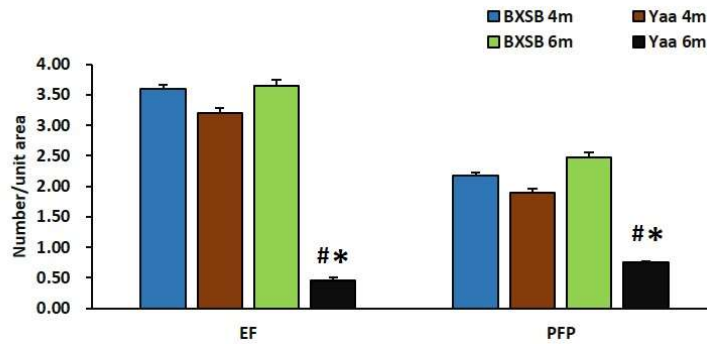
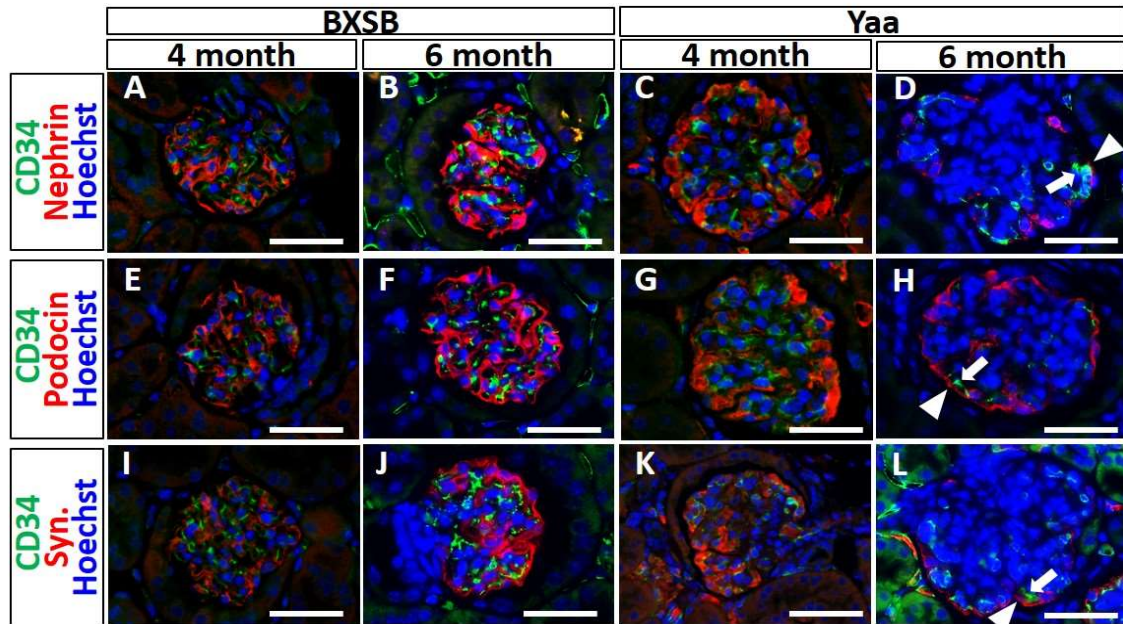**Figure 1-5. Injury of glomerular capillary and podocyte in Yaa mice.**
(A-D) Glomerular capillary and podocyte injury, mSEM. There are well-distributed glomerular capillary EFs (arrowheads) and PFPs (white arrows) in BXSB mice at 4 and 6 months of age (A and B). Normal glomerular capillary EFs (arrowheads), mild PFPs effacement (white arrowheads), and GBM thickening with hump (dashed area) are found in glomerulus of Yaa mice at 4 months of age (C). GBM thickening (two headed arrows) with electron dense materials deposits (arrows), thickened endothelial cytoplasm with loss of EFs (tailed arrows), and PFP effacement (white arrowheads) are found in Yaa mice at 6 months of age (D). Bars = 5 μm.
(E-H) Injury of capillary and podocyte, SEM. There are normal glomerular capillary EFs (arrowheads) in BXSB mice at 4 and 6 months of age (E and F) and in Yaa mice at 4 months of age (G), but loss of EF number (tailed arrows) is observed in glomerular capillary of Yaa mice at 6 months of age (H). There are normal PFPs (white arrows) in BXSB mice at 4 and 6 months of age (I and J). Yaa mice at 4 months of age show microvillus-like structure protruding from podocyte and mild PFPs effacement (K), and Yaa mice at 6 months of age show numerous microvillus-like structures and severe PFP effacement (white arrowheads) (L). Bars = 5 μm.

(M) Number of EFs and PFPs in 4- and 6-month-old BXSB and Yaa glomerulus. Values = mean ± standard error (s.e.) Values = mean ± standard error (s.e.). [#]: Significant difference from the control at the same age, Mann-Whitney U test ([#]$P <$ 0.05). [*]: Significant difference from other groups, Kruskal-Wallis test followed by Scheffe's method ([*]$P < 0.05$); N = 4.

BXSB: BXSB/MpJ, Yaa: BXSB/MpJ-*Yaa*, TEM: transmission electron microscopy, mSEM: modified scanning electron microscopy, SEM: scanning electron microscopy, GBM: glomerular basement membrane, EF: endothelial fenestration and PFP: podocyte foot process.
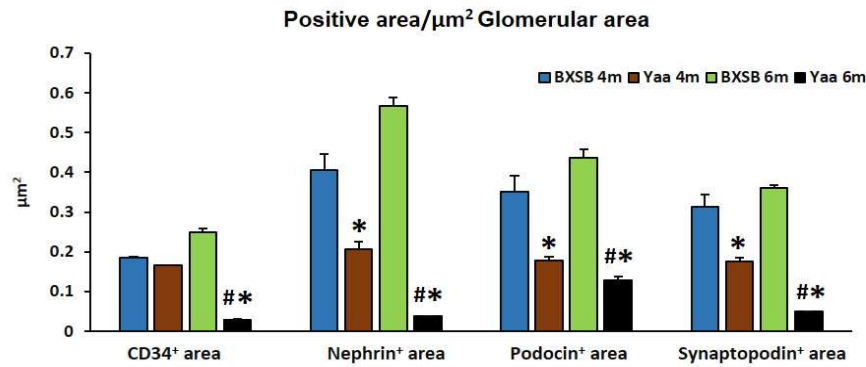
Figure 1-6. Loss of glomerular capillary and podocyte function molecules in Yaa mice

(A-L) Endothelial cell marker (CD34) and podocyte function molecules (Nephrin, Podocin, and Synaptopodin), immunofluorescence. CD34-, Nephrin-, Podocin- and Synaptopodin-immunopositive areas are clearly visible in BXSB mice (A and B, E and F, and I and J), but these are slightly faint at the centre of glomerulus of Yaa mice at 4 months of age (C, G and K) and lost in glomerulus of *Yaa* mutants at 6 months of age (D, H and L). Positive reactions for Nephrin, Podocin, and Synaptopodin (D, H and L, arrowheads) remain in the same areas as CD34$^+$ capillary in Yaa mice (arrows). Bars = 50 μm.

(M) Immunopositive area for CD34, Nephrin, Podocin, and Synaptopodin in 4- and 6-month-old BXSB and Yaa mice. Values = mean ± standard error (s.e.). [#]: Significant difference from the control at the same age, Mann-Whitney *U* test ([#]$P < 0.05$). [*]: Significant difference from other groups, Kruskal-Wallis test followed by Scheffe's method ([*]$P < 0.05$); N = 4.

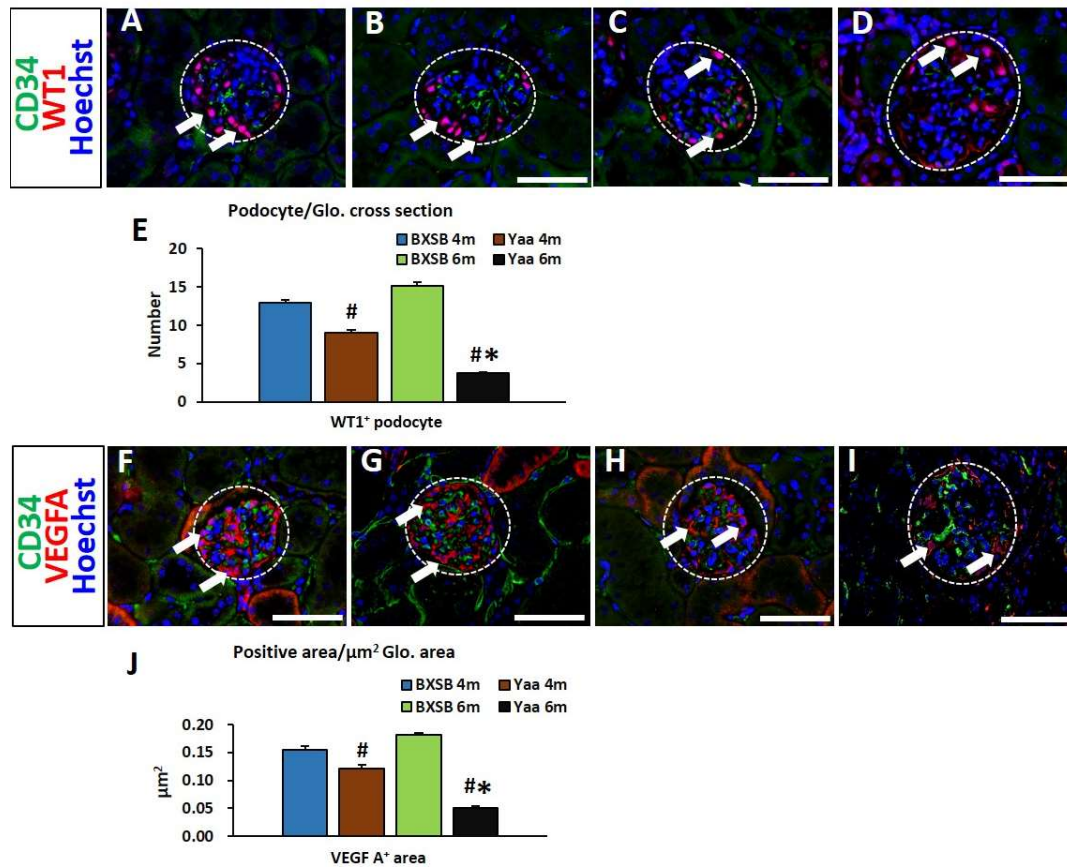BXSB: BXSB/MpJ, Yaa: BXSB/MpJ-*Yaa* and Syn.: Synaptopodin.

Figure 1-7. Loss of podocyte and VEGF A in Yaa mice.

(A-D) CD34^{+} endothelium and WT1^{+} podocytes, immunofluorescence. CD34^{+} capillary and WT1^{+} podocytes are well distributed in BXSB mice at 4 and 6 months of age (A and B). In *Yaa* mutants, WT1^{+} podocytes decrease at 4 months of age (C) but sharply decrease at 6 months of age (D). Bars = 50 μm.

(E) Number of WT1^{+} podocytes in 6-month-old BXSB and Yaa mice. Values = mean ± standard error (s.e [#]: Significant difference from the control at the same age, Mann-Whitney *U* test ([#]$P < 0.05$). [*] Significant difference from other groups, Kruskal-Wallis test followed by Scheffe's method ([*]$P < 0.05$). N = 4.

(F-I) CD34^{+} endothelium and VEGF A^{+} area, immunofluorescence. Normal distribution of CD34- and VEGF A^{+} area is observed in BXSB mice at 4 and 6 months of age (F and G). In Yaa mice, VEGF A[+] areas decrease at 4 and 6 months of age (H and I). Bars = 50 μm.

(J) Measurement of VEGF A[+] area in 4- and 6-month-old BXSB and Yaa mice. Values = mean ± standard error (s.e.). [#]: Significant difference from the control at the same age, Mann-Whitney *U* test ([#]$P < 0.05$). [*]: Significant difference from other groups, Kruskal-Wallis test followed by Scheffe's method ([*]$P < 0.05$); N = 4.

BXSB: BXSB/MpJ, Yaa: BXSB/MpJ-*Yaa*, Glo.: glomerular, VEGF A: vascular endothelial growth factor A and WT1: Wilms tumor 1
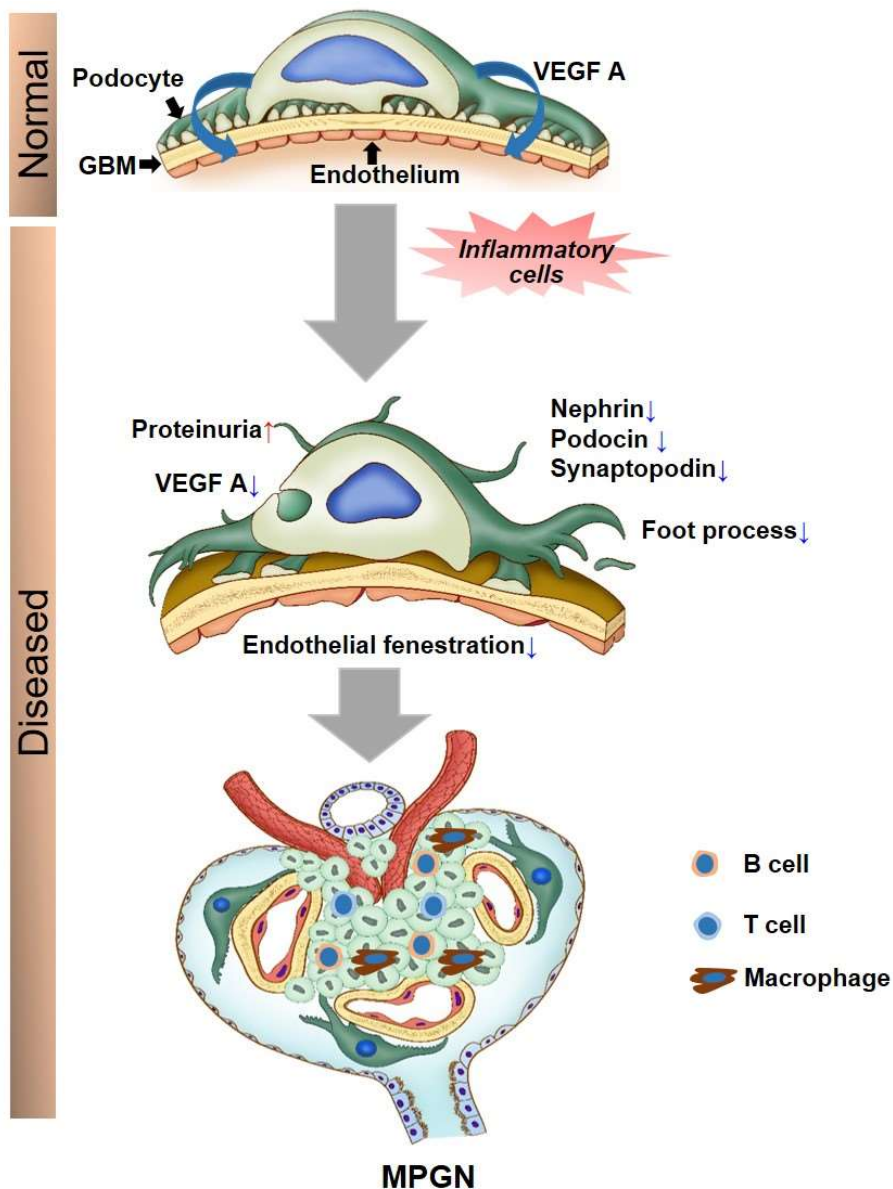
Figure 1-8. Pathological alternations of BUB in the development of AGN.
Podocyte produces VEGF A responsible for maintenance of adjacent endothelium. Increase in inflammatory cells results in podocyte injury, loss of its functional molecules, and proteinuria. Finally, injury and subsequent loss of podocyte results in decreased production of VEGF A that aggravates the endothelial damage and loss of fenestration. Crosstalk between endothelium and podocytes lead to develop AGN.

AGN: autoimmune glomerulonephritis, GBM: glomerular basement membrane and VEGF A: vascular endothelial growth factor A.

Chapter 2

Role of tubulointerstitial blood-urine barrier (BUB)

injury in tubulointerstial lesion development

-Is there any interaction with glomerular BUB?

Introduction

In Chapter 1, the author clarified that ECs and podocytes are crucial cell to maintain BUB integrity in glomerulus and disruption of it leads to GLs. Similarly, the author hypothesized that renal TECs and ECs of PTC form tubulointerstitial BUB which has important role as a barrier between renal tissues and blood stream, and pathological crosstalk between them develop TILs. The author clarified this hypothesis in this Chapter.

CKDs often begin with GLs in which circulating or deposited ICs in glomerulus causes disruption of glomerular BUB components and lead to ultrafiltrations of several proteins and protein-associated factors (Kriz and LeHir, 2005). Chronic GLs are thought to trigger TILs by ultrafiltration of several proteins and inflammatory cytokines (Kriz and LeHir, 2005; Nakai et al., 2006). Finally, chronic GLs progress to ESRD through a common pathway in which progressive tubulointerstitial fibrosis with tubular and PTC damage occur (Kriz and LeHir, 2005).

Renal tubules, comprise about 80% of kidney volume, which are wrapped by PTC and perform many critical renal functions together (Hodgekin and Schnaper, 2012). As the tubulointerstitium has a high demand of energy, they are more susceptible to deprivation of nutrition supply and show TILs. In TILs, injury of PTC network of the kidney is regarded as a key factor (Thomas et al., 1988).

Altered PTC can cause several renal injuries mediated by hypoxia-associated processes (Ohashi et al., 2000; Fine and Norman, 2008; Mayer, 2011). Local hypoxia in the kidney also results in tubular atrophy, inflammation, and interstitial accumulation of extracellular matrix (Fine and Norman, 2008; Mayer, 2011). Loss of VEGF and chronic hypoxia from damaged tubules lead to microvascular dysfunction in kidneys (Nakagawa et al., 2004; Fine and Norman, 2008; Olszewska-Pazdark et al., 2009; Mayer, 2011). Moreover, PTC

ECs have a crucial function in maintaining renal homeostasis and expressing specific chemokines that control compartment-specific T cell and monocyte recruitment during inflammation (Lim et al., 2003; Panzer et al., 2006). This functional variability in ECs is probably associated with differential susceptibilities to apoptosis and differential responses to microenvironmental changes or stimuli. Therefore, injury of tubulointerstitial BUB components, including PTC ECs and TECs, results in TILs. However the crosstalk between PTC ECs and TECs has not been fully elucidated yet.

In this study, the author used mice subjected for unilateral ureteral obstruction (UUO) as TIL model mice. Since other researchers have shown the involvement of renal capillary in the advance of human and experimental animal GN (Shimizu et al., 1997; Takahashi et al., 1998; Kusano et al., 2016), the author also used Yaa mice as GN model to clarify the crosstalk between PTC ECs and TECs in GN.

In Chapter 2, the author clearly elucidated the pathological crosstalk between BUB components, including PTC ECs and TECs, which results in the progression of TILs development. Moreover, the association between glomerular and tubulointersitial BUB was also established in GN model mice.

Materials and Methods

Ethical statements

The author was adhered to ethical guideline during all animal experimentations as described in Chapter 1.

Experimental animal

Six month-old male Yaa mice were used for the GL model, and same-aged male BXSB mice were used as healthy controls. To create the TIL model, eight-week-old male C57BL/6 mice were subjected to UUO for 7 days. The kidney paired with the UUO kidney in the same mouse was used as a normal control. Briefly, mice were deeply anesthetized with a mixture of 0.3 mg/kg medetomidine (Kyoritsu Seiyaku), 4 mg/kg midazolam (Astellas Pharma), and 5 mg/kg butorphanol (Meiji Seika Pharma), and laparotomy in the sublumbar region was performed to ligate the right ureter tightly with silk thread at the renal hilus. Buphrenorphine hydrochloride (Otsuka Pharmaceuticals, Tokyo, Japan) was injected intraperitoneally at a dose rate of 0.3 mg/kg as an analgesic. Recovery from anesthesia was facilitated by intraperitoneal administration of 0.3 mg/kg atipamezole (Zenoaq, Tokyo, Japan).

Sample preparation, serum and urine analysis, and electron microscopy

These methods were performed as described in Chapter 1.

Histopathological examination

Histopathological examinations using PAS-H and PAM technique was performed as described in chapter 1. Immunodetection of different cell markers was performed

according to the procedures shown in Table 2-1.

Histoplanimetry

Digital images of over 30 tubulointerstitial areas randomly selected from each mouse were obtained at 400× magnification using an All-in-One Fluorescence Microscope BZ-X710 (Keyence). The number of CD34$^+$ capillaries observed in the digital images of glomeruli were counted using immunohistochemical sections and a BZ-X Analyzer (Keyence). Further, glomerular damage was semi-quantitatively scored according to methods described by Ichii et al. (Ichii et al., 2008). For TILs, the numbers of B220$^+$ B cells, CD3$^+$ T cells and IL-1F6/IL 36α$^+$ damaged tubules throughout the cortex were counted. Additionally, CD34$^+$ PTC, Iba1$^+$ macrophages, and αSMA$^+$ reaction areas in the tubulointerstitium were counted using immunohistochemical sections and a BZ-X Analyzer (Keyence), based on digital images of the renal cortex.

Visualization of the renal vasculature

After euthanasia, rubber (Microfil, Flow Tech, Inc. Massachusetts, USA) was perfused through left ventricles according to a method described by Walker et al. (Walker et al., 2011). Then, dissected kidneys were fixed with 4% PFA in 0.1 M PB overnight at 4°C. Fixed kidneys were cut into 200-μm-thick sections using a microslicer (DSK Microslicer DTK-3000, Ted Pella, Inc. California, USA) and hydrated with an ascending series of alcohols. Finally, thick sections were cleared with methyl salicylate and examined under a BZ-X Analyzer of an All-in-One Fluorescence Microscope BZ-X710 (Keyence) to obtain Z-stack images.

Statistical analysis

The results were expressed as the mean ± standard error. Statistical analysis was performed as described in Chapter 1.

Results

TILs in GL and TIL models

In the GL model, Yaa mice clearly developed GN as well as TIL characterized by glomerular hypertrophy, increase in glomerular cell number, dilatation of tubules, presence of urinary cast in tubules, infiltrating cells in tubulointerstitial spaces , whereas control BXSB mice did not show any lesion (Fig. 2-1A). No obvious GLs were observed in the TIL model, but UUO kidneys showed severe TILs characterized by dilated tubules with urinary casts, dilation of renal tubular lumens, and immune cell infiltrations in the tubulointerstitium (Fig. 2-1A). Numerous $B220^+$ B cells, $CD3^+$ T cells, and $Iba1^+$ macrophages were observed in TILs of Yaa mice and UUO kidney compare to their respective controls (Fig. 2B-D). In quantitative analysis, significant number of B cells, T cells and macrophages were found in the TILs of Yaa mice and UUO kidney, relative to those in the control kidneys (Fig. 2-1E). With MT staining (Fig. 2-1F), aniline blue-positive sclerotic and fibrotic lesions were observed in GLs of Yaa mice and TILs of UUO kidneys, respectively, but these were not found in their respective controls.

CD34 immunostaining revealed positive reactions in the capillary endothelium of glomerulus and in the tubulointerstitium (Fig. 2-2A). The localizations and intensities of $CD34^+$ PTC were not comparable between Yaa and BXSB mice. However, UUO kidneys showed a decreased number and intensity of $CD34^+$ reactions in TILs. Interestingly, CD34− capillaries, capillaries with lumens that showed no CD34+ staining, were also found in UUO kidneys. In control kidneys for GL and TIL model, $CD34^+$ PTCs were observed clearly in both the glomerulus and tubulointerstitium.

IL-1F6/IL-36$^+$ tubules were detected in TILs as it shows its immunoexpression on damaged renal tubules (Ichii et al., 2010). The author observed, IL-1F6/IL-36$^+$ tubules

were more in Yaa mice and UUO kidney compare to control kidney (Fig. 2-2B). As for TIL parameters such as the number of αSMA+ myofibroblasts, and IL-1F6/IL-36α$^+$ damaged renal tubules in the renal cortex, UUO kidneys showed significantly higher values than control kidneys (Fig. 2-2C). Yaa mice also showed significantly higher values for IL-1F6/IL-36α$^+$ damaged renal tubules than BXSB mice (Fig. 2-2C). Further, UUO kidneys showed significantly higher values for αSMA$^+$ myofibroblasts, and IL-1F6/IL-36α$^+$ damaged renal tubules than kidneys in GL mice (Fig. 2-2C). CD34$^+$ PTCs decrease significantly in UUO kidneys compared to others (Fig. 2-2C).

Alterations in glomerular and tubulointerstitial BUB components

In thick sections of rubber-injected kidneys (Fig. 2-3A), alterations in both glomerular and PTCs were not obvious in Yaa and BXSB mice. However, PTCs loss was evident in UUO kidneys, in contrast to control kidneys which showed a fine capillary network.

In ultrastructural observation of the glomerular BUB in both model mice by TEM, thickened glomerular capillary endothelium and PFP effacements was observed only in Yaa mice (Fig. 2-3B-a). Other mice showed normal glomerular capillary endothelium and podocyte (Fig. 2-3B-b, c and d).

In ultrastructural observation of the tubulointerstitial BUB in both model mice by TEM, thickened PTC ECs with subendothelial space was observed only in Yaa mice compare to its normal control (Fig. 2-3C-a and b). However, in the TIL model, PTC injuries were clearly observed in UUO kidneys (Fig. 2-3C-c). These injuries were characterized by stratification of thickened endothelial cytoplasms with vacuolation, and wide subendothelial spaces were also found in PTCs (Fig. 2-3C-c). Control kidneys showed normal PTC and TEC (Fig. 2-3C-d).

Correlations between the number of CD34+ capillaries and histopathological indices in GL and TIL models

The number of $CD34^+$ PTC was significantly and negatively correlated with the number of infiltrating $B220^+$ B cells, $CD3^+$ T cells, $Iba1^+$ macrophages, IL-1F6/IL-36α^+ damaged renal tubules, and αSMA^+ myofibroblasts in the TILs of TIL model mice (Table 2-2), but only with infiltrating $CD3^+$ T-cells and $Iba1^+$ macrophages in GL model mice (Table 2-2). As both GLs and TILs were observed in GL model mice only, the author performed correlation analysis between indices for GLs and TILs. The author found that number of $CD34^+$ PTC and IL-1F6/IL-36α^+ damaged renal tubules were significantly correlated with indices for GLs, including glomerular damage score, uACR, $CD34^+$ glomerular capillary, $WT1^+$ podocyte, in GL model mice (Table 2-3).

Discussion

BUB components, including PTC and TEC, are essential for renal oxygen supply and maintenance of kidney tubulointerstitial hemodynamics (Kang et al., 2002; Nangaku, 2004). It has been indicated that TILs activate the endothelium, which may correlate with enhanced inflammation and activation of coagulation that favors further capillary and interstitial injury (Pichler et al., 1995; Ishidoya et al., 1996). Eventually, persistent TILs cause a loss of PTC (Nicolic-Paterson et al., 1994). In the present study, TIL models were created by UUO. TILs model mice clearly showed a decrease in CD34^{+} PTC with the progression of TILs, characterized by an increase in infiltrating cells and myofibroblasts, as well as damaged tubules in the tubulointerstitium. Furthermore, the ultrastructural study revealed capillary injuries in TILs in detail. These injuries were characterized by thickened and stratified endothelial cytoplasm with vacuolation, loss of fenestration, and detaching endothelia with subendothelial vacuolation. Thus, our results clearly indicate pathological correlations between TILs and PTC injury and/or loss in tubulointerstitium in UUO-based TIL models.

In particular, the number of infiltrating CD3^{+} T cells strongly correlated with the number of CD34^{+} PTC in TILs of UUO models. Therefore, the author presumed that interstitial T cells mediate inflammation and the accumulation of macrophages in the tubulointerstitium. Importantly, an increase in Iba-1^{+} macrophages significantly correlated with a decrease in CD34^{+} PTC in the present study. Another study showed that apoptosis of ECs triggered capillary regression by blocking blood flow to the site of apoptosis in macrophage-dependent cell death (Meeson et al., 1996). Renal fibrosis results from reduced endothelial proliferation following alterations in local expression of both angiogenic and antiangiogenic factors, and this imbalance is mediated by

46

macrophage-associated cytokines, such as interleukin 1 beta (IL-1β), and vasoactive mediators (Kang et al., 2002). Based on these findings, the author considered tubulointerstitial inflammation, especially macrophage infiltration underlie the injury of capillary ECs and the subsequent net loss of capillaries.

The present study revealed a significant correlation between the number of CD34^{+} PTC and the numbers of IL-1F6/IL-36α^{+} damaged renal tubules in UUO kidney. Evidently, loss of PTC caused TILs because of local hypoxia, because PTC and renal tubules show functional crosstalk to maintain normal renal interstitial structure and function, including preserving the blood supply to maintain TECs. This speculation is strongly supported by previous study indicating that renal ischemia caused by vascular obliteration is a major contributor to renal fibrosis (Fine and Norman, 2008). Moreover, the TECs are source of VEGF in the tubulointerstitium (Schrijvers et al., 2004). Therefore, the author concluded that injury and/or loss of PTC contribute to the progression of tubular damage and vice-versa.

The Yaa mouse is a model of spontaneous AGN, with hyperproliferation of pathogenic B cells resulting from a Yaa mutation that contributes to autoantibody production, activation of pathogenic T cells, and secretion of pro-inflammatory cytokines that contribute to the development of GLs (Ichii et al., 2008 and 2010; Bekar et al., 2010; Kimura et al., 2011; Nowling and Gilkeson, 2011). Importantly, the author showed the positive correlation between damaged renal tubules and glomerular histopathological indices. Therefore, the author considered that GL events appear earlier and were severer than TILs in Yaa mice. However, glomerular efferent arterioles directly connect to branches of PTC, a reduction in blood supply to the glomerulus might affect TILs. Further, no significant GLs were noted in UUO models. Importantly, number of CD34^{+} PTC didn't

significantly changed between BXSB and Yaa mice, but correlated with infiltrating T cells and macrophages in TILs. The author hypothesized that loss of $CD34^+$ PTC didn't occur drastically in Yaa mice but change in capillary endothelial structure and immunogenicity would contribute to TILs in Yaa mice which is clarified in next Chapter.

Furthermore, podocyte injury is a critical event that causes albumin hyperfiltration from glomerular capillaries (Kimura et al., 2013). Indeed, the author showed PFP effacement in GL model mouse kidneys, but not in those of the TIL model mouse. Thus, pathological changes in the glomerular microenvironment resulting from injury of podocytes and capillary endothelia coordinately aggravate GLs and lead to an elevation in uACR. The present study revealed a significant correlation between the numbers of IL-1F6/IL-36α^+ damaged renal tubules and uACR in GL model. Moreover, $CD34^+$ PTC was correlated with glomerular damage score, $CD34^+$ glomerular capillary and $WT1^+$ podocyte number. Therefore, the author speculated that injury of glomerular BUB injury leads to proteinuria which in turn affects tubulointerstitial BUB components and results in TILs in GL model.

Thus, in Chapter 2, the author elucidated the pathological crosstalk between TECs and PTCs in TILs progression. In addition, defective interactions between glomerular and tubulointerstitial BUB in GL model was clearly revealed. A close correlation between the number of inflammatory cells in the kidney and the injury of glomerular and tubulointerstitial BUB was found in first two chapters. Therefore, the author focused on the BUB component as an immunological candidate in next Chapter.

Summary

In the previous Chapter, the author elucidated the pathological crosstalk between components of glomerular BUB. In Chapter 2, the author revealed tubulointerstitial BUB which composed of renal TECs and ECs of PTC, and pathological crosstalk between them developed into TILs.

UUO-treated TIL model mice showed severe TILs and decreased CD34$^+$ PTCs compared to those in untreated control kidneys. However, Yaa, the GL model mice developed severe GLs and TILs, and the number of CD34$^+$ PTC was comparable between BXSB and Yaa mice. Infiltrations of B cells, T cells, and macrophages increased significantly in the respective lesions of both disease models. IL-1F6/IL-36α$^+$ damaged renal tubules also increased in TILs of both model mice kidney. In observations of microfil rubber-perfused thick kidney sections by fluorescence microscopy, segmental absences of PTCs were observed in TILs of UUO-treated mice only. Further, TEM revealed tubulointerstitial BUB injury in TIL model, and both glomerular and tubulointerstitial BUB injury in GL model mice kidney. The numbers of CD34$^+$ PTCs significantly and negatively correlated with the number of all examined indices for TILs in TIL model mice, but only with those in infiltrating CD3$^+$ T cells and Iba1$^+$ macrophages in GL model mice. Moreover, CD34$^+$ PTC in GL model mice was correlated with indices for GLs in GL model mice.

In Chapter 2, the author clearly revealed the pathological crosstalk between tubulointerstitial BUB components, which results in TILs development. Moreover, the author also emphasized the association between glomerular and tubulointersitial BUB in GL model mice.

Tables and Figures

Table 2-1. Summary of immunostaining conditions.

	αSMA	CD34	IL-1F6/IL-36α
Antigen retrieval	CB 105°C, 20 min	CB 105°C, 20 min	CB 105°C, 20 min
Blocking	10% NGS	10% NGS	5% NDS
Primary antibody	Rabbit polyclonal antibodies (Abcam, Cambridge, UK) 1:3000	Rat polyclonal antibodies (Abcam, Cambridge, UK) 1:400	Goat polyclonal antibodies (R&D Systems, Minnesota, USA) 1:400
Biotinylated secondary antibody	Goat anti-rabbit (SABPO kit, Nichirei, Tokyo, Japan) 1:100	Goat anti-rat IgG (Caltag Medsystems, Buckingham, UK) 1:100	Donkey anti-goat IgG (Santa Cruz, California, USA) 1:100

CB: citrate buffer, NGS: normal goat serum and NDS: normal donkey serum

Table 2-2. Correlation between CD34$^+$ PTC and histopathological parameters of TILs in

GL and TIL model mice.

CD34$^+$ PTC		Indices for Ti. histopathology				
		Ti. B220$^+$ B cells	Ti. CD3$^+$ T cells	Ti. Iba1$^+$ macrophages	IL-1F6/IL-36α$^+$ renal tubules	Ti. αSMA$^+$ myofibroblasts
GL model	ρ	-0.130	-0.813*	-0.786*	-0.683	-
	P	0.456	0.0102	0.002	0.060	-
TIL model	ρ	-0.857**	-0.970**	-0.857**	-0.913**	-0.905**
	P	0.007	0.001<	0.007	0.002	0.002

*P < 0.05 and **P < 0.01, Spearman's correlation coefficient; N = 8 (Diseased and respective control). Ti.: tubulointerstitial, GLs: glomerular lesions, TILs: tubulointerstitial lesions, IL-1F6: interleukin 1 family, member 6 and -: not determined;

Table 2-3. Correlation between indices for GL and TIL in GL model mice.

		Glo. damage score	uACR	CD34$^+$ Glo. capillary	WT1+ Pod.
CD34+ PTC	ρ	-0.950**	-0.641	0.880**	0.812*
	P	0.001	0.083	0.004	0.015
IL-1F6/IL-36α$^+$ renal tubules	ρ	0.875**	0.907**	-0.905**	-0.781*
	P	0.004	0.002	0.002	0.050

*$P < 0.05$ and **$P < 0.01$, Spearman's correlation coefficient; N = 8 (BXSB and Yaa). Glo.: glomerular, Pod.: podocyte, uACR: urinary albumin-to-creatinine ratio, GL: glomerular lesion, PTC: peritubular capillary, -: not determined, BXSB: BXSB/MpJ and Yaa: BXSB/MpJ-*Yaa*.
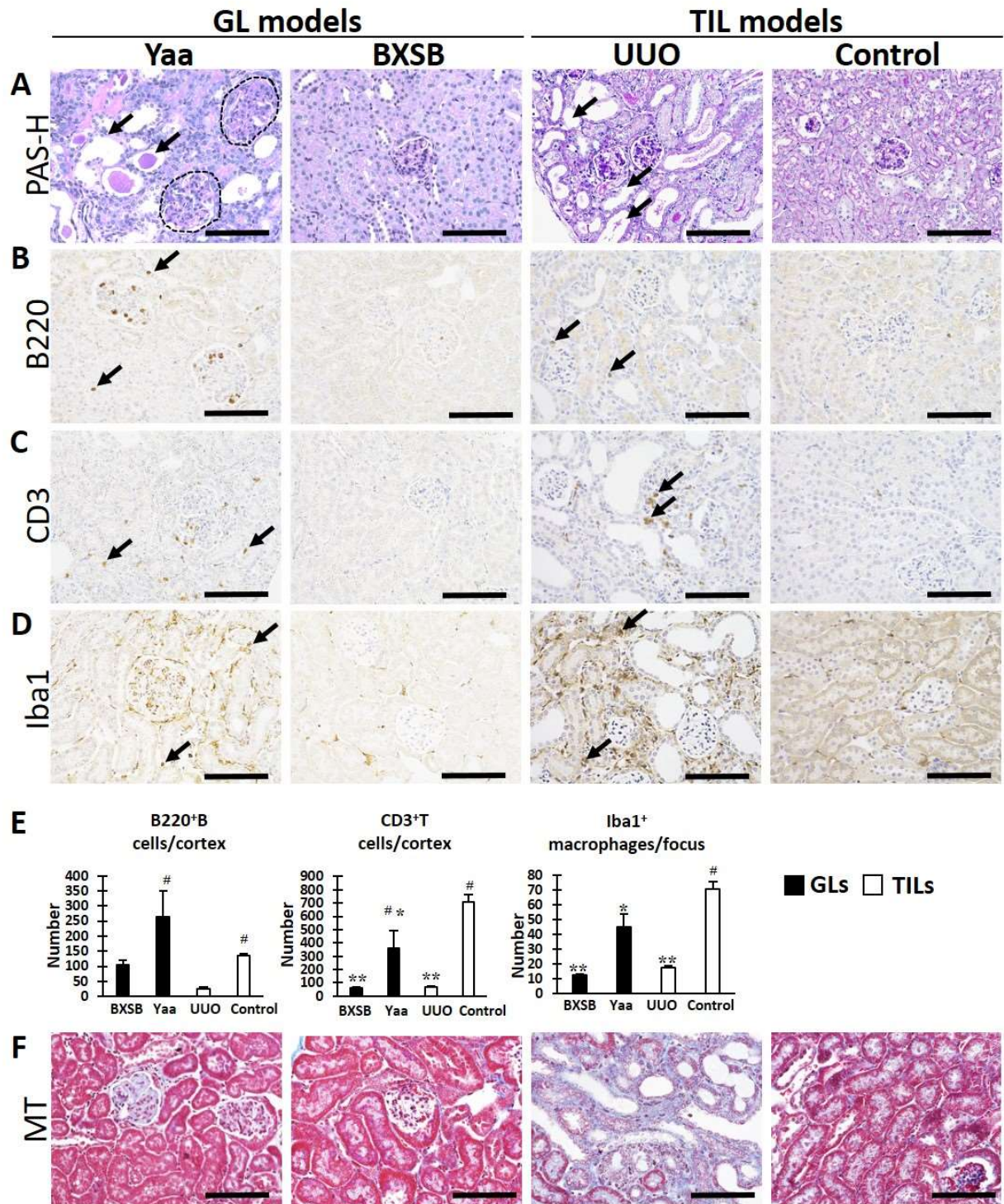
Figure 2-1. GLs and TILs in GL and TIL mouse models.
(A) GLs (dashed area) and TILs (arrow) in Yaa (GL model) and UUO kidney (TIL model) and, their respective controls. PAS-H staining. All bars = 100 µm.

(B–D) Analysis of B220$^+$ B cell, CD3$^+$ T cells, and Iba-1$^+$ macrophage infiltration in TILs of Yaa mice and UUO mice and, their respective controls. Immunohistochemistry.

(E) Indices for the number of infiltrating B220$^+$ B cells, CD3$^+$ T cells, and Iba1$^+$ macrophages in the model mice. $^\#$: Significant difference from the control at the same age, Mann-Whitney U test ($^\#P < 0.05$). *: Significant difference from other groups, Kruskal-Wallis test followed by Scheffe's method ($^*P < 0.05$, $^{**}P < 0.01$); N = 4. a, b, c, and d denote BXSB, Yaa, Control, and UUO kidney, respectively.

(F) Evaluations of renal fibrosis in the kidneys of Yaa mice and UUO kidney and, their respective controls. MT staining. All bars = 100 µm.

GLs: glomerular lesions, TILs: tubulointerstitial lesions, PAS-H: periodic acid Schiff-hematoxylin, MT: Masson's trichrome, BXSB: BXSB/MpJ, Yaa: BXSB/MpJ-*Yaa* and UUO: unilateral ureteral obstruction.
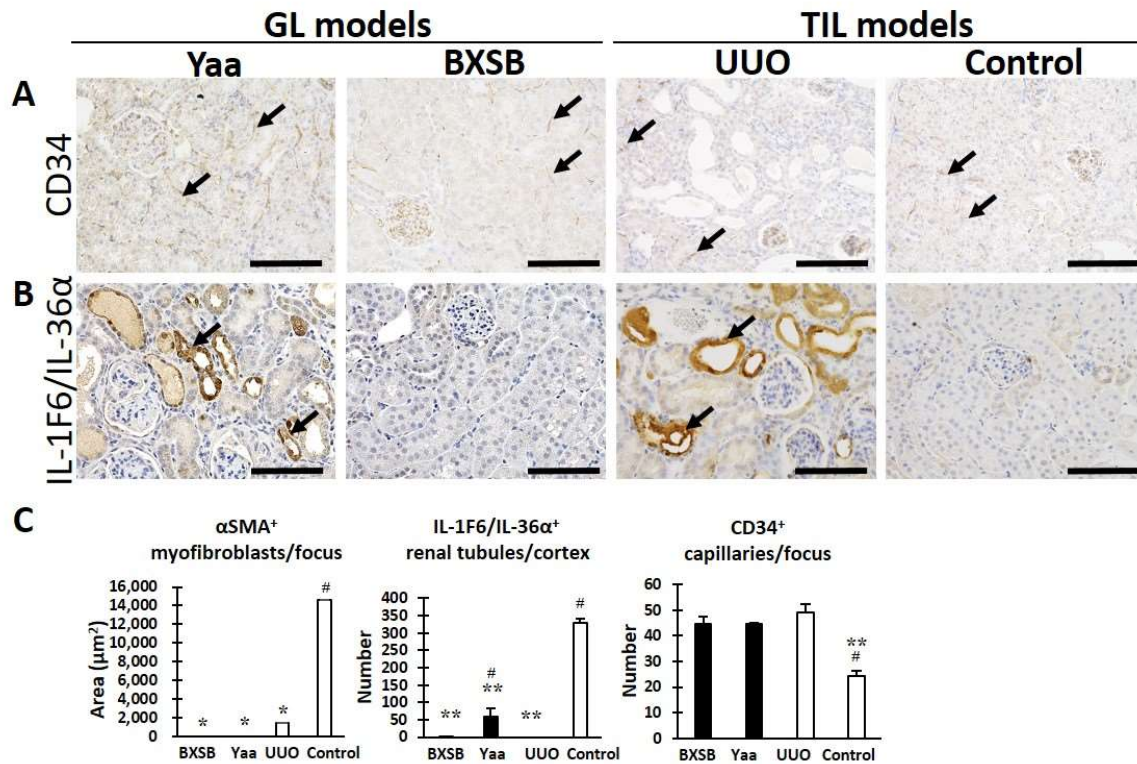
Figure 2-2. PTC and TEC injury-associated histological parameters in both GL and TIL models.

(A) Analysis of CD34$^+$ cells in Yaa mice and UUO kidney and, their respective controls. Immunohistochemistry. All bars = 100 μm.

(B) IL-1F6/IL-36α$^+$ damaged tubules in Yaa mice and UUO kidney and, their respective controls. Immunohistochemistry. All bars = 100 μm.

(C) Indices for tubulointerstitial damage, including the area of αSMA$^+$ myofibroblasts and the number of IL-1F6/IL-36α$^+$ damaged tubules and CD34$^+$ capillaries in the model mice.

$^{\#}$: Significant difference from the control at the same age, Mann-Whitney U test ($^{\#}P < 0.05$).

*: Significant difference from the other groups, Kruskal-Wallis test followed by Scheffe's method ($^{*}P < 0.05$, $^{**}P < 0.01$); N = 4. a, b, c, and d denote BXSB, Yaa, Control, and UUO kidney, respectively. GL: glomerular lesion, TIL: tubulointerstitial lesion, BXSB: BXSB/MpJ, Yaa: BXSB/MpJ-*Yaa*, UUO: unilateral ureteral obstruction and IL-1F6: interleukin-1 family, member 6.
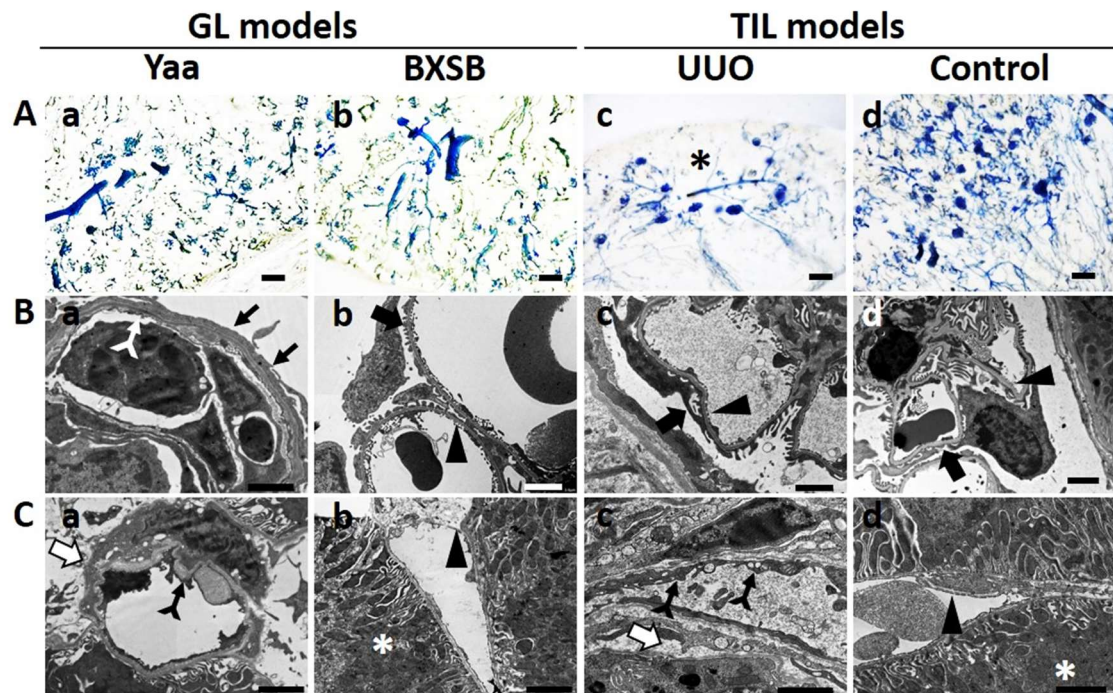
Figure 2-3. Structural alterations in BUB of model mice.
(A) Capillary structures in the kidneys of Yaa mice (a), UUO kidney (c), and their respective controls (b and d), visualized in thick kidney section following by rubber perfusion. Bars = 200 μm. Asterisks indicate segmental loss of PTCs.
(B) Ultrastructures of glomerular BUB in model mice by TEM. Thickened glomerular capillary endothelium (white tailed arrow) and PFP effacement (thin black arrow) in Yaa mice (panel a). Glomerular capillary endothelium (black arrowhead) and podocytes (thick black arrow) are well preserved in BXSB mice, UUO kidney and its collateral control kidney (panel b, c and d). All bars = 2 μm.
(C) Ultrastructures of tubulointerstitial BUB in model mice by TEM. Thickened PTC endothelial cytoplasm (black tailed arrow) with subendothelial space (thick empty arrow) in Yaa mice (panel a). Normal PTC endothelial cytoplasm (black arrowhead) and TEC (white asterisks) in BXSB mice (panel b). Thickened and stratified endothelial cytoplasm in PTC of UUO kidney (black tailed arrows) with subendothelial space (thick empty arrow) (panel c). Control kidneys shows normal PTC endothelial cytoplasm (black arrowhead) and TEC (white asterisks) (panels d). All bars = 2 μm.

GL: glomerular lesion, TIL: tubulointerstitial lesion, BXSB: BXSB/MpJ, Yaa: BXSB/MpJ-*Yaa*, UUO: unilateral ureteral obstruction, BUB: blood-urine barrier, TEM: transmission electron microscopy, PTC: peritubular capillary, TEC: tubular epithelial cell, and PFP: podocyte foot process.

Conclusion

In recent years, increasing number of human and companion animal suffering from chronic kidney disease (CKD) has been considered as global concern as it is associated with cardiovascular complications as well as end-stage renal disease. Therefore, early diagnosis and therapeutics intervention is important to fill up the target of 'Zoobiquity'. Importantly, most of the CKD showed injury of blood-urine barrier (BUB) components irrespective of their etiologies. So, understanding the pathobiology of the BUB is invaluable for the development of better diagnostic and therapeutic strategies to reduce incidence of CKD. In this thesis, the author clarified the effects of injured BUB components and their achieved function as immunological gateway during CKD development.

In Chapter 1, the author evaluated pathological crosstalk between components of the glomerular BUB in the development of CKD. BXSB/MpJ-Yaa (Yaa) was used as CKD model mouse due to autoimmune glomerulonephritis. Similar to transmission electron microscopy (TEM), modified scanning electron microscopy (mSEM) revealed pathological changes in glomerular BUB components of Yaa mice compare to its control BXSB/MpJ (BXSB). Further, immunopositive area of endothelium and podocyte functional molecules significantly decreased in Yaa compared with BXSB. The indices

of glomerular endothelial cells (ECs) and podocyte injuries were significantly correlated with each other and with indices of autoimmune disease and renal dysfunction. Thus, the author elucidated the pathological crosstalk between ECs and podocytes in CKD progression and the usefulness of mSEM for pathological analysis.

In chapter 2, tubulointerstitial BUB consisting of renal tubular epithelial cells and peritubular capillary (PTC) ECs as well as glomerular BUB has been investigated using two CKD model mice. In addition to Yaa, unilateral ureteral obstruction (UUO) model was used as tubulointerstitial lesion (TIL) model of CKD. Both Yaa and UUO model showed TILs. TEM analysis showed injury of both glomerular and tubulointerstitial BUB injury in Yaa and only tubulointerstitial BUB injury in UUO kidney. Furthermore, the number of CD34 positive PTC in the UUO kidney was significantly and negatively correlated with all the measured TIL indexes. On the other hand, Yaa negatively correlated with tubulointerstitial inflammation index and glomerular injury index. These data strongly suggested that injury of tubulointerstitial BUB constituents are involved in TIL progression of CKD and that glomerular BUB and tubulointerstitial BUB are pathologically related to each other.

Recent studies stated that BUB components are recognized as active participants in the innate immune response. In Chapter 3, the authors focused on Toll like receptor 9 (TLR

9), an innate immune response-related molecule, in the activation of different BUB components and subsequent development of lesions in CKD. Yaa mice showed strong expression of *Tlr9* mRNA and protein in podocyte and PTC ECs as well as increased level of mRNA expression for *Tlr9* and its putative downstream cytokines in isolated glomeruli and tubulointerstitium compare to BXSB. From the above, it can be considered that in CKD, the increase in TLR9 expression in podocytes and ECs of PTC are involved in each cell injury and lesion formation. In addition, mSEM analysis revealed injury of BUB constitutive cells in Yaa glomerulus and tubulointerstitium.

In conclusion, the author clarified the molecular pathogenesis of CKD and considered that injury of BUB components is critical in progression of glomerular lesion and TIL. The author clarified pathological crosstalk between BUB components and also between glomerular and tubulointersitial BUB in CKD. Moreover, the author strongly believes that TLR9 could be used as diagnostic and therapeutic target as it showed its adverse effects on different components of BUB during CKD development.

References

1   Abrass, C.K., Berfield, A.K., Ryan, M.C., Carter, W.G., and Hansen, K.M. 2006. Abnormal development of glomerular endothelial and mesangial cells in mice with targeted disruption of the lama3 gene. *Kidney Int.*, **70**: 1062–1071.

2   Akira, S., Takeda, K., and Kaisho, T. 2001. Toll-like receptors: Critical proteins linking innate and acquired immunity. *Nat. Immunol.*, **2**: 675–680.

3   Anders, H.J., Banas, B., Linde, Y., Weller, L., Cohen, C.D., Kretzler, M., Martin, S., Vielhaur, V., Schlondorff, D., and Grone, H.J. 2003. Bacterial CpG-DNA aggravates glomerulonephritis: role of TLR9-mediated expression of chemokines and chemokine Receptors. *J. Am. Soc. Nephrol.*, **14**: 317–326.

4   Baccala, R., Gonzalez-Quintial, R., Lawson, B.R., Stern, M.E., Kono, D.H., Beutler, B., and Theofilopoulos, A.N. 2009. Sensors of the innate immune system: their mode of action. *Nat. Rev. Rheumatol.*, **5**: 448–456.

5   Ballermann, B. J. Glomerular endothelial cell differentiation. 2005. *Kidney Int.,* **67**: 1668–1671.

6   Banas, M.C., Banas, B., Hudkins, K.L., Wietecha, T.A., Iyoda, M., Bock, E., Hauser, P., Pippin, J.W., Shankland, S.J., Smith, K.D., Stoelcker, B., Liu, G., Gröne,

H.J., Krämer, B.K., and Alpers, C.E. 2008. TLR4 links podocytes with the innate immune system to mediate glomerular injury. *J. Am. Soc. Nephrol.*, **19**: 704–713.

7   Bartlett, P.C., Van Buren, J.W., Bartlett, A.D., and Zhou, C. 2010. Case-control study of risk factors associated with feline and canine chronic kidney disease. *Vet. Med. Int.*, **2010**: 957570.

8   Bekar, K.W., Owen, T., Dunn, R., Ichikawa, T., Wang, W., Wang, R., Barnard, J., Brady, S., Nevarez, S., Goldman, B.L., Kehry, M., and Anolik, J.H. 2010. Prolonged effects of short-term anti-CD20 B cell depletion therapy in murine systemic lupus erythematosus. *Arthr. Rheum.*, **62**: 2443–2457.

9   Benigni, A., Caroli, C., Longaretti, L., Gagliardini, E., Zoja, C., Galbusera, M., Moioli, D., Romagnani, P., Tincani, A., Andreoli, L., and Remuzzi, G. 2007. Involvement of renal tubular Toll-like receptor 9 in the development of tubulointerstitial injury in systemic lupus. *Arthritis Rheuma.*, **56**: 1569–1578.

10   Breier, G., Albrecht, U., Sterrer, S., and Risau, W. 1992. Expression of vascular endothelial growth factor during embryonic angiogenesis and endothelial cell differentiation. *Development,* **114**: 521–532.

11 Chan, O.T., Hannum, L.G., Haberman, A.M., Madaio, M.P., and Shlomchik, M.J. 1999. A novel mouse with B cells but lacking serum antibody reveals an antibody independent role for B cells in murine lupus. *J. Exp. Med.* **189**: 1639–1648.

12 Cheng, H., and Harris, R.C. 2014. Renal endothelial dysfunction in diabetic nephropathy. *Cardiovasc. Hematol. Disord. Drug Targ.*, **14**: 22–33.

13 Conti, F., Spinelli, F.R., Truglia, S., Miranda, F., Alessandri, C., Ceccarelli, F., Bombardieri, M., Giannakakis, K., and Valesini, G. 2016. Kidney expression of toll like receptors in lupus nephritis: quantification and clinicopathological correlations. *Mediators Inflamm.*, **2016**: 7697592.

14 Coresh J, Astor BC, Greene T, Eknoyan, G., and Levey, A.S. 2003. Prevalence of chronic kidney disease and decreased kidney function in the adult US population: Third National Health and Nutrition Examination Survey. *Am. J. Kidney Dis.*, **41**: 1-12.

15 Curry, F.E. and Adamson, R.H. 2012. Endothelial glycocalyx: permeability barrier and mechanosensor. *Ann. Biomed. Eng.*, **40**: 828–839.

16 D'Agati, V.D., Kaskel, F.J.and Falk, R.J. 2011. Focal segmental glomerulosclerosis. *N. Engl. J. Med.*, **365**: 2398–2411.

17 Daehn, I., Casalena, G., Zhang, T., Shi, S., Fenninger, F., Barasch, N., Yu, L., D'Agati, V. D., Schlondorff, D., Kriz, W., Haraldsson, B., and Bottinger, E.P. 2014. Endothelial mitochondrial oxidative stress determines podocyte depletion in segmental glomerulosclerosis. *J. Clin. Invest.*, **124**: 1608–1621.

18 Eleftheriadis, T., Pissas, G., Liakopoulos, V, Stefanidis, I., and Lawson, B.R. 2012. Toll-like receptors and their role in renal pathologies. *Inflamm. Allergy Drug Target*, **11**: 464–477.

19 Endemann, D.H., and Schiffrin, E.L. 2004. Endothelial dysfunction. *J. Am. Soc. Nephrol.*, **15**: 1983–1992.

20 Eremina, V., Sood, M., Haigh, J., Nagy, A., Lajoie, G., Ferrara, N., Gerber, H.P., Kikkawa, Y., Miner, J.H., and Quaggin, S.E. 2003. Glomerular-specific alterations of VEGF-A expression lead to distinct congenital and acquired renal diseases. *J. Clin. Invest.* **111**: 707–716.

21 Fine, L.G., and Norman, J.T. 2008. Chronic hypoxia as a mechanism of progression of chronic kidney diseases: from hypothesis to novel therapeutics. *Kidney Int.*, **74**: 867–872.

22 Frey, N., and Olson, E.N. 2003. Cardiac hypertrophy: the good, the bad, and the ugly. *Annu. Rev. Physio.*, **65**: 45–79.

23 Garraud, O., and Cognasse, F. 2010. Platelet Toll-like receptor expression: the link between ''danger'' ligands and inflammation. *Inflamm. Allergy Drug Targets*, **9**: 322–333.

24 Gorden, K.K., Qiu, X.X., Binsfeld, C.C., Vasilakos, J.P., and Alkan, S.S. 2006. Cutting edge: activation of murine TLR8 by a combination of imidazoquinoline immune response modifiers and polyT oligodeoxynucleotides. *J. Immunol.* **177**: 6584–6587.

25 Gurkan, S., Cabinian, A., Lopez, V., Bhaumik, M., Chang, J.M., Rabson, A.B., and Mundel, P. 2013. Inhibition of type I interferon signaling prevents TLR ligand mediated proteinuria. *J. Pathol.*, **231**: 248–256.

26 Haraldsson, B., Nystrom, J., and Deen, W.M. 2008. Properties of the glomerular barrier and mechanisms of proteinuria. *Physiol. Rev.* **88**: 451–487.

27 Hodgkins, K.S. and Schnaper, H.W. 2012. Tubulointerstitial injury and the progression of chronic kidney disease. *Pediatr Nephrol.*, **27**: 901-909.

28 Ichii, O., Konno, A., Sasaki, N., Endoh, D., Hashimoto, Y., and Kon, Y. 2008. Altered balance of inhibitory and active Fc gamma receptors in murine autoimmune glomerulonephritis. *Kidney Int.,* **74**: 339–347.

29 Ichii, O., Konno, A., Sasaki, N., Endoh, D., Hashimoto, Y., and Kon, Y. 2010. Autoimmune glomerulonephritis induced in congenic mouse strain carrying telomeric region of chromosome 1 derived from MRL/MpJ. *Histol. Histopathol.*, **23**: 411–422.

30 Isermann, B., Vinnikov, I.A., Madhusudhan, T., Herzog, S., Kashif, M., Blautzik, J., Corat, M.A., Zeier, M., Blessing, E., Oh, J., Gerlitz, B., Berg, D.T., Grinnell, B.W., Chavakis, T., Esmon, C.T., Weiler, H., Bierhaus, A., and Nawroth, P.P. 2007. Activated protein C protects against diabetic nephropathy by inhibiting endothelial and podocyte apoptosis. *Nat. Med.* **13**: 1349–1358.

31 Ishidoya, S., Morrisey, J., McCracken, R., and Klahr, S. 1996. Delayed treatment with enalapril halts tubulointerstitial fibrosis in rats with obstructive nephropathy. *Kidney Int.*, **49**: 1110–1119.

32 Kang, D.H., Kanellis, J., Hugo, H., Truong, L., Anderson, S., Kerjaschki, D., Schreiner, G.F., and Johnson, R.J. 2002. Role of the microvascular endothelium in progressive renal disease. *J. Am. Soc. Nephrol.*, **13**: 806–816.

33 Khakpour, S., Wilhelmsen, K., and Hellman, J. 2015. Vascular endothelial cell toll-like receptor pathways in sepsis. *Innate Immunol.*, **21**: 827–846.

34 Kida, Y., Tchao, B.N., and Yamaguchi, I. 2014. Peritubular capillary rarefaction: a new therapeutic target in chronic kidney disease. *Pediatr. Nephrol.*, **29**: 333–342.

35 Kimura, J., Ichii, O., Otsuka, S., Kanazawa, T., Namiki, Y., Hashimoto, Y., and Kon, Y. 2011. Quantitative and qualitative urinary cellular patterns correlate with progression of murine glomerulonephritis. *PLoS One*, **6**: e16472.

36 Kimura, J., Ichii, O., Otsuka, S., Sasaki, H., Hashimoto, Y., and Kon, Y. 2013. Close relations between podocyte injuries and membranous proliferative glomerulonephritis in autoimmune murine models. *Am. J. Nephrol.*, **38**: 27–38.

37 Kimura, J., Ichii, O., Miyazono, K., Nakamura, T., Horino, T., Otsuka-Kanazawa, S., and Kon, Y. 2014. Overexpression of Toll-like receptor 8 correlates with the progression of podocyte injury in murine autoimmune glomerulonephritis. *Sci. Rep.*, **4**: 7290.

38 Kobayashi N, Ueno T, Ohashi K, Yamashita H, Takahashi Y, Sakamoto K, Manabe, S., Hara, S., Takashima, Y., Dan, T., Pastan, I., Miyata, T., Kurihara, H., Matsusaka, T., Reiser, J., and Nagata, M. 2015. Podocyte injury-driven intracapillary plasminogen activator inhibitor type 1 accelerates podocyte loss via uPAR-mediated β1-integrin endocytosis. *Am. J. Physiol. Renal. Physiol.*, **308**: F614–F626.

39 Koga, D., Kusumi, S., Shodo, R., Dan, Y., and Ushiki, T. 2015. High-resolution imaging by scanning electron microscopy of semi thin sections in correlation with light microscopy. *Microscopy (Oxf),* **64**: 387–394.

40 Kramann, R., Kusaba, T., and Humphreys, B.D. 2015. Who regenerates the kidney? *Nephrol. Dial. Transplant.*, **30**: 903-910.

41 Kriz, W., and LeHir, M. 2005. Pathways to nephron loss starting from glomerular diseases-insights from animal models. *Kidney Int.*, **67**: 404-419.

42 Kriz, W., Gretz, N., and Lemley, K. V. 1998. Progression of glomerular diseases: is the podocyte the culprit? *Kidney Int.*, **54**: 687–697.

43 Kusano, T., Takano, H., Kang, D., Nagahama, K., Aoki, M., Morita, M., Kaneko, T., Tsuruoka, S., and Shimuzu, A. 2016. Endothelial cell injury in acute and chronic glomerular lesions in patients with IgA nephropathy. *Hum. Pathol.*, **49**: 135–144.

44 Leadbetter, E.A., Rifkin, I.R., Hohlbaum, A.M., Beaudette, B.C,, Shlomchik, M.J., and Marshak-Rothstein, A. 2002. Chromatin-IgG complexes activate B cells by dual engagement of IgM and Toll-like receptors. *Nature*, **416**: 603–607.

45 Lim, Y.C., Garcia-Cardena, G., Allport, J.R., Zervoglos, M., Connolly, A.J., Gimbrone Jr, M.A., and Luscinskas, F. W. 2003. Heterogeneity of endothelial cells

from different organ sites in T-cell subset recruitment. *Am. J. Pathol.*, **162**: 1591–1601.

46 Lindenmeyer, M.T., Kretzler, M., Boucherot, A., Berra, S., Yasuda, Y., Henger, A., Eichinger, F., Gaiser, S., Schmid, H., Rastaldi, M.P. Schrier, R.W. Schlondorff, D., and Cohen, C.D. 2007. Interstitial vascular rarefaction and reduced VEGF-A expression in human diabetic nephropathy. *J. Am. Soc. Nephrol.*, **18**: 1765–1776.

47 Liu, B., Tang, T., Lv, L., and Lan, H. 2018. Renal tubule injury: a driving force toward chronic kidney disease. *Kidney Int.*, **93**: 568–579.

48 Lysaght, M.J. 2002. Maintenance dialysis population dynamics: current trends and long-term implications. *J. Am. Soc. Nephrol.*, **13**: S37-S40.

49 Machida, H., Ito, S., Hirose, T., Taleshita, F., Oshiro, H., Nakamura, T., Mori, M., Inayama, Y., Yan, K., Kobayashi, N., and Yokota, S. 2010. Expression of Toll-like receptor 9 in renal podocytes in childhood-onset active and inactive lupus nephritis. *Nephrol. Dial. Transplant.*, **25**: 2530–2537.

50 Mayer, G. 2011. Capillary rarefaction, hypoxia, VEGF and angiogenesis in chronic renal disease. *Nephrol. Dial. Transplant.*, **26**: 1132–1137.

51 Means, T.K., Latz, E., Hayashi, F., Murali, M.R., Golenbock, D.T., and Luster, A.D. 2005. Human lupus autoantibody-DNA complexes activate DCs through cooperation of CD32 and TLR9. *J. Clin. Invest.*, **115**: 404-417.

52 Meeson, A., Palmer, M., Calfon, M., and Lang, R. 1996. A relationship between apoptosis and flow during programmed capillary regression is revealed by vital analysis. *Development*, **122**: 3929–3938.

53 Menon, M.C., Chuang, P.Y. and He, C.J. 2012. The glomerular filtration barrier: components and crosstalk. *Int. J. Nephrol.*, **2012**: 749010.

54 Nagata, M. 2016. Podocyte injury and its consequences. *Kidney Int.*, **89**: 1221–1230.

55 Nagata, M., Ninomiya, T., Doi, Y., Yonemoto, K., Kubo, M., Hata, J., Tsuruya, K., Iid,a M., and Kiyohara, Y. 2010. Trends in the prevalence of chronic kidney disease and its risk factors in a general Japanese population: the Hisayama Study. *Nephrol. Dial. Transplant*, **25**: 2557–2564.

56 Nakagawa, T., Lan, H.Y., Zhu, H.J., Kang, D.H., Schreiner, G.F., and Johnson, R.J. 2004. Differential regulation of VEGF by TGF-beta and hypoxia in rat proximal tubular cells. *Am. J. Physiol. Renal. Physiol.*, **287**: F658–F664.

57 Nakai, S., Wada, A., Kitaoka, T., Shinzato, T., Nagura, Y., Kikuchi, K., Masakane, I., Shinoda, T., Yamazaki, C., Sakai, R., Marubayashi, S., Morita, O., Iseki, K.,

Usami, T., Kimata, N., Suzuki, K., Tabei, K., Fushimi, K., Miwa, N., Yauchi, M., Wakai, K., and Akiba, T. 2006. An overview of regular dialysis treatment in Japan. *Ther. Apher. Dial.*, **10**: 476-497.

58 Nangaku, M. 2004. Mechanisms of tubulointerstitial injury in the kidney: Final common pathways to end-stage renal failure. *Intern. Med.*, **43**: 9–17.

59 Nicolic-Paterson, D.J., Lan, H.Y., and Atkins, R.C. 1994. Macrophages in renal injury. *Kidney Int. Suppl.*, **45**: S79-S82.

60 Nihalani, D., and Susztak, K. 2013. Sirt1-Claudin-1 crosstalk regulates renal function. *Nat. Med.*, **19**:1371–1382.

61 Nikolic-Paterson, D.J. and Atkins, R.C. 2001. The role of macrophages in glomerulonephritis. *Nephrol. Dial. Transplant.*, **16**: 3–7.

62 Nowling, T.K., and Gilkeson G.S. 2011. Mechanisms of tissue injury in lupus nephritis. *Arthritis Res. Ther.*, **13**: 250.

63 Ohashi, R., Kitamura, H., and Yamanaka, N. 2000. Peritubular capillary injury during the progression of experimental glomerulonephritis in Rats. *J. Am. Soc. Nephrol.*, **11**: 47–56.

64 Ohashi, R., Shimizu, A., Masuda, Y., Kitamura, Y., Ishizaki, M., Sugisaki, Y., and Yamanaka, N. 2002. Peritubular capillary regression during the progression of experimental obstructive nephropathy. *J. Am. Soc. Nephrol.*, **13**: 1795–1805.

65 Olszewska-Pazdrak, B., Hein, T.W., Olszewska, P., and Carney, D.H. 2009. Chronic hypoxia attenuates VEGF signaling and angiogenic responses by downregulation of KDR in human endothelial cells. *Am. J. Physiol. Cell Physiol.*, **296**: C1162–C1170.

66 Orikasa, M., Matsui, K., Oite, T. and Shimizu, F. 1998. Massive proteinuria induced in rats by a single intravenous injection of a monoclonal antibody. *J. Immunol.*, **141**: 807–814.

67 Panzer, U., Steinmetz, O.M., Reinking, R.R., Meyer, T.N., Fehr, S., Schneider, A., Zahner, G., Wolf, G., Helmchen, U., Schaerli, P., Stahl, R.A. and Thaiss, F. 2006. Compartment-specific expression and function of the chemokine IP-10/CXCL10 in a model of renal endothelial microvascular injury. *J. Am. Soc. Nephrol.*, **7**: 454–464.

68 Papadimitraki, E.D., Tzardi, M., Bertsias, G., Sotsiou, E., and Boumpas, D.T. 2009. Glomerular expression of toll-like receptor-9 in lupus nephritis but not in normal kidneys: implications for the amplification of the inflammatory response. *Lupus,* **18**: 831–835.

69 Patole, P.S., Pawar, R.D., Lech, M., Zecher, D., Schmidt, H., Segerer, S., Ellwart, A., Henger, A., Kretzler, M., and Anders, H.J. 2006. Expression and regulation of toll-like receptors in lupus-like immune complex glomerulonephritis of MRL fas (lpr) mice. *Nephrol. Dial. Transplant.*, **21**:3062–3073.

70 Pichler, R.H., Franceschini, N., Young, B.A., Hugo, C., Andoh, T.F., Burdmann, E.A., Shankland, S.J. Alpers, C.E. Bennet, W.M., and Couser, W.G. 1995. Pathogenesis of cyclosporine nephropathy: Roles of angiotensin II and osteopontin. *J. Am. Soc. Nephrol.*, **6**: 1186–1196.

71 Roselli, S. Heidet, L., Sich, M., Henger, A., Kretzler, M., Gulber, M.C., and Antignac, C. 2004. Early glomerular filtration defect and severe renal disease in podocin-deficient mice. *Mol. Cell Biol.*, **24**: 550–560.

72 Saleem, M.A., O'Hare, M.J., Reiser, J, Coward, R.J., Inward, C.D., Farren, T., Xing, C.Y., Ni, L., Mathieson, P.W., and Mundel, P. 2002. A conditionally immortalized human podocyte cell line demonstrating nephrin and podocin expression. *J. Am. Soc. Nephrol.*, **13**: 630–638.

73 Salvador, B., Arranz, A., Francisco, S., Córdoba, L., Punzón, C., Llamas, M.A., and Fresno, M. 2016. Modulation of endothelial function by Toll like receptors. *Pharmacol. Res.*, **108**: 46-56.

74 Santiago-Raber, M.L., Laporte, C., Reininger, L. and Izui, S. 2004. Genetic basis of murine lupus. *Autoimmun. Rev.,* **3**: 33–39.

75 Satchell, S.C. and Braet, F. 2009. Glomerular endothelial cell fenestrations: an integral component of the glomerular filtration barrier. *Am. J. Physiol. Renal. Physiol.,* **296**: F947–F956.

76 Schrijvers, B.F., Flyvbjerg, A., and De Vriese, A.S. 2004. The role of vascular endothelial growth factor (VEGF) in renal pathophysiology. *Kidney Int.,* **265**: 2003–2017.

77 Scott, R.P. and Quaggin, S.E.2015. Review series: the cell biology of renal filtration. *J. Cell Biol.,* **209**: 199–210.

78 Segelmark, M., and Helmark, T. 2010. Autoimmune kidney diseases. *Autoimmun. Rev.,* 9: A366-A371.

79 Shimizu, A., Kitamura, H., Masuda, Y., Ishizaki, M., Suqisak, Y., and Yamanaka, N. 1997. Rare glomerular capillary regeneration and subsequent capillary regression with endothelial cell apoptosis in progressive glomerulonephritis. *Am. J. Pathol.,* **151**: 1231–1239.

80 Shirali, A.C., and Goldstein, D.R. 2008. Tracking the Toll of Kidney Disease. *J. Am. Soc. Nephrol.,* **19**: 1444–1450.

81 Sivaskandarajah, G.A., Jeansson, M., Maezawa, Y., Eremina, V., Baelde, H.J., and Quaggin, S.E. 2012. Vegfa protects the glomerular microvasculature in diabetes. *Diabetes,* **61**: 2958-2955.

82 Smyth, L.J., Duffy, S., Maxwell, A.P., and McKnight, A.J. 2014. Genetic and epigenetic factors influencing chronic kidney disease. *Am. J. Physiol. Renal Physiol.,* **307**: F757-F776.

83 Soares, A.A., Prates, A.B., Weinert, L.S., Veronese, F.V., de Azevedo, M.J., and Silveiro, S.P. 2013. Reference values for glomerular filtration rate in healthy Brazilian adults. *BMC Nephrol.,* **14**: 54.

84 Stillman, I.E. and Karumanchi, S.A. 2007. The glomerular injury of preeclampsia. *J. Am. Soc. Nephrol.,* **18**: 2281–2284.

85 Subramanian, S., Tus, K., Li, Q.Z., Wang, A., Tian, X.H., Zhou, J., Liang, C., Bartov, G., McDaniel, L.D., Zhou, X.J., Schultz, R.A., and Wakeland, E.K. 2006. A Tlr7 translocation accelerates systemic autoimmunity in murine lupus. *Proc. Natl. Acad. Sci., U S A.,* **103**: 9970–9975.

86 Takahashi, T., Huynh-Do, U., and Daniel, T.O. 1998. Renal microvascular assembly and repair: power and promise of molecular definition. *Kidney Int.,* **53**: 826–835.

87 Takemoto, M., Asker, N., Gerhardt, H., Lundkvist, A., Johansson, B.R., Saito, Y., and Betsholtz, C. 2002. A new method for large scale isolation of kidney glomeruli from mice. *Am. J. Pathol.*, **161**: 799–805.

88 Tang, R., Han, Y., Wu, M., Zhu, D., and Liu, B. 2014. The effects of endothelial injury in renal fibrosis progression. *Aust. J. Nephrol. Hypertens.*, **1**: 1021.

89 Thomas, S.E., Anderson, S., Gordon, K.L., Oyama, T.T., Shankland, S.J,, and Johnson, R.J. 1988. Tubulointerstitial disease in aging: Evidence of underlying peritubular capillary damage, potential role for renal ischemia. *J. Am. Soc. Nephrol.*, **9**: 231–242.

90 Tonelli, M., Wiebe, N., Culleton, B., House, A., Rabbat, C., Fok, M., McAlister, F., and Garg, A.X. 2006. Chronic kidney disease and mortality risk: a systematic review. *J. Am. Soc. Nephrol.*, **17**: 2034–2047.

91 Toyoda, M., Najafian, B., Kim, Y., Caramori, M.L., and Mauer, M. 2007. Podocyte detachment and reduced glomerular capillary endothelial fenestration in human type 1 diabetic nephropathy. *Diabetes*, **56**: 2155– 2160.

92 Tsuboi, N., Yoshikai, Y., Matsuo, S., Kikuchi, T., Iwami, K., Nagai, Y., Takeuchi, O., Akira, S., and Matsuguchi, T. 2002. Roles of toll-like receptors in C-C chemokine production by renal tubular epithelial cells. *J. Immunol.*, **169**: 2026–2033.

93 Unnersjö-Jess, D., Scott, L., Blom, H., and Brismar, H. 2016. Super-resolution stimulated emission depletion imaging of slit diaphragm proteins in optically cleared kidney tissue. *Kidney Int.*, **89**: 243–247.

94 Vedulla, M., Alonso, J.L., Arnaout, M.A., and Charest, J.L. 2017. A microfluidic renal proximal tubule with active reabsorptive function. *PLoS One,* **12**: e0184330.

95 Walker, E.J., Shen, F., Young, W.L., and Su, H. 2011. Cerebrovascular casting of the adult mouse for 3D imaging and morphological analysis. *J. Vis. Exp.*, **30**: e2958.

96 Weil, E.J., Lemley, K.V., Mason, C.C., Yee, B., Jones, L.I., Blouch, K., Lovato, T., Richardson, M., Myers, B.D., and Nelson, R.G. 2012. Podocyte detachment and reduced glomerular capillary endothelial fenestration promote kidney disease in type 2 diabetic nephropathy. *Kidney Int.*, **82**, 1010–1017.

97 Xia, H., Bao, W., and Shi, S. 2017. Innate Immune Activity in Glomerular Podocytes. *Front. Immunol.*, **8**: 122.

98 Yi, F., dos Santos, E.A., Xia, M., Chen, Q.Z., Li, P.L., and Li, N. 2007. Podocyte injury and glomerulosclerosis in hyperhomocysteinemic rats. *Am. J. Nephrol.*, **27**: 262–268.

Acknowledgement

Conclusion in Japanese

　近年、動物およびヒト共に慢性腎臓病（CKD）の症例数が増えている。本症は心血管疾患リスクを増加させ、その進行は透析を必要とする末期腎不全（ESRD）を導くため、CKD 症例数の増加は世界的に深刻な問題である。それ故、本症の早期診断と治療は"汎動物科学的観点"からも重要な課題である。重要なことに、多くの CKD は血液尿関門（BUB）の構成要素を障害するため、その病理機序の解明はより有効な CKD 制御に繋がると考えられる。本学位論文では、著者は CKD 進行における BUB 構成要素の傷害とその病理学的な影響を明らかにした。さらに、BUB 構成要素は局所の免疫学的ゲートとして機能することを示した。

　第 1 章では、糸球体 BUB 構成要素の病理学的クロストークを評価した。BXSB/MpJ-Yaa (Yaa)を自己免疫性糸球体腎炎（AGN）に起因する CKD モデルマウスとして用いた。透過型電子顕微鏡（TEM）解析は BUB 構成要素である足細胞の超微細構造学的な細胞傷害を明らかに示した。また、独自の病理解析手法として改変走査型電子顕微鏡（mSEM）解析を応用し、TEM 同様、足細胞傷害を可視化した。さらに、Yaa 糸球体における足細胞機能関連分子や血管内皮細胞マーカー分子の発現は健常対照 BXSB/MpJ（BXSB）よりも有意に減弱した。また、糸球体の足細胞と血管内皮細胞の細胞傷害指標は互いに相関し、それらは自己免疫異常および腎機能悪化の指標とも相関した。以上より、著者は AGN に起因した CKD における BUB 構成要素、特に足細胞と血管内皮細胞の病理学的クロストークを示した。また、その評価における mSEM 解析の有用性を示した。

　著者は第 2 章において、糸球体 BUB 同様、尿細管間質にも尿細管上皮細胞と周囲の血管内皮細胞から成る BUB が存在し、それらの病理学的クロストークは尿細管間質障害（TIL）に関連し、CKD 進行に寄与する可能性を考えた。Yaa に加え、本章では CKD における TIL モデルとして尿管結紮(UUO)モデルを用いた。Yaa および UUO モデル共に尿細管上皮細胞傷害や間質の炎症を伴う TIL を示した。TEM 解析において、両モデル共に尿細管周囲の血管内皮細胞に細胞傷害像がみられた。さらに、UUO モデルの尿細管周囲 CD34 陽性血管内皮細胞数は計測した全て TIL 指標と有意に負の相関を示した。一方、Yaa のそれは尿細管間質の炎症指標および糸球体傷害指標と負に相関した。以上、本結果は CKD の TIL 進行に尿細管間質 BUB 構成要素の傷害が深く関与すること、また糸球体 BUB と尿細管間質 BUB は病理学的に相互に関与することを強く示唆した。

　近年、BUB 構成細胞は自然免疫応答を介して腎障害プロセスに関与することが示唆されて

いる。第 3 章では、著者は自然免疫応答関連分子である Toll like receptor 9 (TLR9)に着目し、Yaa を用いて CKD におけるその発現動態と BUB の関連性を評価した。TLR9 の mRNA と蛋白は足細胞と尿細管周囲の血管内皮細胞に局在し、それらの発現は BXSB よりも Yaa で強かった。分離した糸球体および尿細管間質における TLR9 およびその下流分子候補の mRNA 発現量は BXSB よりも Yaa で高かった。分離した糸球体および尿細管間質における TLR9 の mRNA 発現量は各組織傷害スコアおよび局所の下流分子候補の mRNA 発現量と有意に相関した。また、mSEM 解析で Yaa の糸球体および尿細管間質における BUB 構成細胞の細胞傷害を明らかにした。以上より、CKD において、足細胞と尿細管周囲の血管細胞における TLR9 発現の増加は各々の細胞傷害と病変形成に関与すると考えらえた。

　結論として、著者は CKD の分子病態を解析し、BUB 構成要素の傷害が糸球体および尿細管間質の障害に深く関与することを示し、また BUB 構成要素間および糸球体と尿細管間質の BUB 間における病理学的クロストークを明らかにした。特に TLR9 は CKD 進行時の各 BUB 障害に深く関与するため、新たな診断ならびに治療のターゲットとして興味深い。